Accepted Manuscript

Constraining magma storage conditions using phase equilibria models at a restless volcano in the Main Ethiopian Rift

Matthew L.M. Gleeson, Michael J. Stock, David M. Pyle, Tamsin A. Mather, William Hutchison, Gezahegn Yirgu
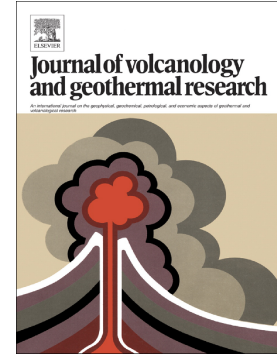
Please cite this article as: Matthew L.M. Gleeson, Michael J. Stock, David M. Pyle, Tamsin A. Mather, William Hutchison, Gezahegn Yirgu , Constraining magma storage conditions using phase equilibria models at a restless volcano in the Main Ethiopian Rift. The address for the corresponding author was captured as affiliation for all authors. Please check if appropriate. Volgeo(2017), doi: 10.1016/j.jvolgeores.2017.02.026

Original Manuscript

Constraining magma storage conditions using phase equilibria models at a restless volcano in the Main Ethiopian Rift

Matthew L. M. Gleeson[1,2]*, Michael J. Stock[1,2], David M. Pyle[1], Tamsin A. Mather[1], William Hutchison[1,3] and Gezahegn Yirgu[4]

[1]Department of Earth Sciences, University of Oxford, South Parks Road, Oxford OX1 3AN, UK.

[2]Department of Earth Sciences, University of Cambridge, Downing Street, Cambridge CB2 3EQ, UK.

[3]Department of Earth Sciences and Environmental Sciences, University of St Andrews, North Street, St Andrews, KY16 9AL, UK

[4] School of Earth Sciences, Addis Ababa University, P.O. Box 1176, Addis Ababa, Ethiopia

ABSTRACT

The Main Ethiopian Rift hosts a number of peralkaline volcanic centres, with many showing signs of recent unrest. Due, in part, to the low number of historical eruptions recorded in the region, volcanism in the Main Ethiopian Rift remains understudied relative to other volcanic settings and conditions of magma storage remain almost entirely unknown. Aluto is one of these restless caldera systems and identifying magma storage conditions is vital for evaluating the risks posed by recent periods of unrest. In this study, we ran ~150 fractional crystallisation models, using the Rhyolite-MELTS thermodynamic software, within the range P = 50 – 300 MPa, starting H_2O = 0.5 – 3 wt% and fO_2 = QFM-2 – QFM+1. This represents a realistic range of potential magma storage conditions at Aluto. We assessed the fractionation trends produced using two different starting compositions, which represent different estimates of the parental melt feeding the system. The predicted liquid lines of descent produced by these models are compared with Aluto whole-rock data from the literature, and are presented along with new observations of the natural phase assemblage and erupted mineral compositions to provide information on the magma storage conditions.

Original Manuscript

Using a new, quantitative statistical approach to compare empirical data and thermodynamic model-outputs, we find that the compositions of evolved peralkaline rhyolites from Aluto are best reproduced by isobaric fractional crystallisation from a rift-related basaltic composition, without the need for significant crustal assimilation. Around 90% protracted fractional crystallisation is required to produce these compositions. This indicates that the magmatic system is likely to exist as a highly crystalline mush. The best agreement between models and natural samples is at low pressures (150 MPa), low initial H_2O concentrations (0.5 wt%) and relatively high oxygen fugacity (QFM). The depth of magma storage derived from these results (~5.6 ± 1 km) agrees well with the source depths modelled from measured ground deformation at Aluto in 2008. Data from other peralkaline volcanic centres in the Main Ethiopian Rift, such as Boset and Gedemsa, and at other locations globally (e.g. Pantelleria, Italy) suggest that these storage conditions are a common feature of many peralkaline volcanic centres. Our data is consistent with the formation of a Daly Gap at Aluto due to compositional stratification of the magma reservoir beneath the caldera, and the non-linear relationship between temperature and SiO_2 concentration during magmatic differentiation.

Highlights:

- Rhyolite-MELTS is used to evaluate magma storage conditions, and a novel statistical approach is used to quantitatively compare model outputs with empirical datasets.

- Isobaric fractional crystallisation of a basaltic parental magma can reproduce the pantelleritic compositions of eruptive products from Aluto.

- The storage conditions under which the geochemistry of Aluto eruptive products are best reproduced by Rhyolite-MELTS models are: fO_2 = QFM; P = 150 MPa; initial H_2O = 0.5 wt%.

- Magmatic storage in the shallow crust (~5.6 ± 1 km) is in good agreement with modelling of InSAR observations that suggests shallow crustal magmatic activity at Aluto (5.1 ± 0.5 km).

- The Daly Gap at Aluto is formed due to a combination of density stratification of the magma reservoir and the scarcity of intermediate products produced by fractional crystallisation.

Original Manuscript

- The magma storage conditions determined for Aluto are similar to those at similar volcanic centres in MER and other peralkaline volcanoes worldwide (e.g. Boset, Gedemsa, and Pantelleria).

Key Words: Rhyolite-MELTS; Magma storage; Aluto; Main Ethiopian Rift; Daly Gap

1 INTRODUCTION

At the northern end of the East African Rift system, the active Main Ethiopian Rift (MER) and the Afar Depression represent two distinct stages in the transition from a continental rift to a slow-spreading 'oceanic' rift (Ebinger, 2005). In the MER, volcanic features include both focussed, caldera-forming silicic centres, and elongate rift-controlled basaltic fields, dominantly composed of monogenetic centres (Abebe et al., 2007; Corti, 2009). Volcanic activity is generally concentrated within localised segments, controlled by dense fault swarms (Corti, 2009). In the Afar region, incipient seafloor spreading centres characterise the initiation of the Red Sea Rift, with extension largely accommodated by dikes (Wright et al., 2006; Keir et al., 2009), which are indicative of a more mature rift-setting.

In this study, we investigate the magmatic evolution of Aluto volcano, Ethiopia. Aluto is a young peralkaline silicic volcano located in the MER. Aluto has been active for >300 ka and underwent a phase of major caldera forming volcanism at ~310, post caldera volcanism has taken place since 60 ka and is dominated by the eruption of evolved peralkaline rhyolites (Hutchison et al., 2015, 2016a,b,c). Aluto is also one of a number of prominent restless caldera systems in the MER, showing evidence for recent ground deformation (Biggs et al., 2011; Hutchison et al., 2016a), and hosts an important hydrothermal system (Hutchison et al., 2015). Hydrothermal systems such as this offer geothermal resources that may provide significant economic benefits for Ethiopia (Kebede, 2012; Younger, 2014). Evaluating the potential risks associated with developing geothermal energy plants on these restless volcanic systems requires investigation of the magma storage conditions during the

Original Manuscript

most recent eruptive periods. Improving our understanding of how and where magmas evolve beneath peralkaline volcanic centres is particularly important, given the potential hazards posed by the infrequent explosive eruptions at these volcanic systems. Aluto is a suitable target for this study as it is currently showing signs of unrest (Biggs et al., 2011; Hutchison et al., 2016a), and recent geophysical observations allow comparison of the present magmatic activity with that inferred for past eruptive episodes.

We explore the hypothesis that the composition of the volcanic products at Aluto can be generated by closed-system, isobaric fractional crystallisation (i.e. without crustal assimilation) and aim to determine the conditions of magma storage before recent eruptions. We approach this by calculating potential liquid lines of descent across a wide range of potential magmatic storage conditions (i.e. pressure, oxygen fugacity [fO_2], initial H_2O content) using the Rhyolite-MELTS thermodynamic modelling software (Gualda et al., 2012) and comparing model outputs with whole rock compositions of natural samples. We develop a statistical test to quantitatively assess the 'fit' between modelled liquid lines of descent, and empirical whole rock data. On identifying the 'best case' magma storage conditions (i.e. the model parameters that best predict the natural melt compositions), we compare these petrological constraints with the interpreted depth of melt accumulation from geophysical measurements of recent ground deformation, and seismic activity, at Aluto. Comparison between current activity and petrologically derived magma storage conditions of past eruptions has not previously been attempted at Aluto and may provide important information regarding the potential scale and eruptive style of future activity.

1.1 Genesis of Peralkaline Magmas

Peralkaline magmas are defined as having a peralkalinity index (molar $(???? + ??)/????$) greater than 1 (Macdonald, 1974), with peralkaline rhyolites further sub-divided into comendites (high Al_2O_3 and low FeO_t) and pantellerites (low Al_2O_3 and high FeO_t). Peralkaline magmas occur globally and are commonly associated with ocean islands (e.g. Socorro Island, Mexico; Bohrson and Reid, 1997),

Original Manuscript

localised extension in collisional settings (e.g. Pantelleria; White et al., 2009) and continental rifts (e.g. Gedemsa; Peccerillo et al., 2003). Isotopic and trace element analysis of peralkaline volcanic products suggests that fractional crystallisation is the dominant mechanism by which peralkaline rhyolites are generated (e.g. Peccerillo et al., 2003; Ronga et al., 2009; LeMasurier et al., 2011; Field et al., 2012; Neave et al., 2012; Rooney et al., 2012), though in some systems (e.g. Gedemsa) radiogenic isotope ratios point to a limited role for crustal contamination (e.g. Davies and Macdonald, 1987; Black et al., 1997; Peccerillo et al., 2003; Giordano et al., 2014).

Experimental data on equilibrium and fractional crystallisation indicates that generation of peralkaline magmas may be favoured by low pressure conditions, characteristic of the upper crust (Caricchi et al., 2006). This experimental data indicates that fractional crystallisation from a transitional basaltic parent cannot produce melt compositions that cross the subaluminous/peralkaline divide at P > 0.5 GPa. Caricchi et al. (2006) suggest that the highly fractured nature of the crust at continental rift settings may allow magma to intrude to shallow crustal levels. This stabilises plagioclase feldspar and inhibits amphibole crystallisation, leading to an increase in the peralkalinity index of the residual melt (Caricchi et al., 2006). Additionally, Scaillet and Macdonald (2003) showed that during crystallisation under relatively reduced conditions (<QFM – Quartz-Fayalite-Magnetite buffer) the peralkalinity of a magma increases as crystallisation of calcic clinopyroxene is inhibited under these conditions. This is in agreement with the study of Scaillet and Macdonald (2001), which showed that the phase relationships of peralkaline rhyolites are consistent with crystallisation at or below the QFM buffer.

2 GEOLOGICAL SETTING

The MER is a ~500 km long zone of active continental rifting between the Nubian and Somalian plates (Fig. 1; Corti, 2009) and is considered a type example of an active continental rift (Ebinger, 2005). It can be split into three sections (the Northern, Central, and Southern MER). These

Original Manuscript

developed diachronously and display significant along-axis variation in structure and morphology (Keir et al., 2015).

The initial Miocene-Pliocene rifting in the MER occurred due to displacement along large boundary faults, resulting in the subsidence of asymmetric basins (Corti, 2009), with relatively diffuse, bimodal volcanism (Abebe et al., 2005). At present, the deformation style changes along the MER as rift maturity increases northward (Agostini et al., 2011); in the Southern MER, active extension is largely controlled by displacement along boundary faults (Corti et al., 2013), whereas, during the Pleistocene, the main boundary faults of the Central MER were deactivated and deformation was localised into dense fault swarms, along en-echelon segments within the thinned rift axis (Corti, 2009; Agostini et al., 2011). These volcano-tectonic segments focussed the ascending magma and corresponding volcanic centres (Ebinger and Casey, 2001). In contrast, the Northern MER is more closely analagous to the Afar region where extension is achieved via dike emplacement, similar to oceanic spreading centres (Ebinger et al, 2010; Ferguson et al., 2013).

2.1 ALUTO

Aluto volcano is located in the Central MER, around 100 km south of Addis Ababa. The complex comprises a 700 m high, 14 km wide edifice predominantly composed of peralkaline pumice cones, ignimbrites, lava flows and domes (Hutchison et al., 2015).

Exploration wells drilled in the 1980s have revealed the underlying crustal structure and volcanic stratigraphy at Aluto (Gianelli and Teklemariam, 1993; Gizaw, 1993). For most of the Pleistocene, volcanic activity was dominated by rift-related basaltic volcanism (Hutchison et al., 2016b). The early Aluto edifice comprises a series of trachytic tuffs and lacustrine sediment that were emplaced before deposition of a thick welded ignimbrite sequence at ~310 ka, which was likely accompanied by caldera collapse. The current (post-caldera) phase of volcanism started at ~60 ka and is characterised by rhyolitic pumice cones and obsidian coulees (Hutchison et al., 2016b). Aluto remains active, with current estimates indicating an eruption rate of 1 every 1000 years in the last 10 ka (Hutchison et al.,

Original Manuscript

2016b). We focus on the on the most recent (i.e. <60 ka) phase of volcanism at Aluto. These erupted products have a narrow compositional range, with many analysed samples classified as pantellerites, according to the scheme of Macdonald (1974). Very few basaltic or intermediate-composition ejecta are known to have erupted within the past 60 ka, and these deposits are confined to a number of small vents located to the NW of the main volcanic complex. Recent vents are largely located along pre-existing faults, including a major NNE-SSW-trending fault zone (the Artu Jawe fault zone [AJFZ]) and a hypothesised ring-fault produced during caldera formation (Hutchison et al., 2015).

Hutchison et al. (2016b) published major and trace element data for a large suite of Aluto samples and compiled whole-rock data from previous studies (Di Paola, 1972; Mamo, 1985; Teklemariam, 1996; Teklemariam et al., 1996; Yimer, 1984). These data are summarised in Table 1, and provide the basis for our geochemical analysis and thermodynamic modelling of magmatic evolution at Aluto. Trace element modelling by Hutchison et al. (2016b) suggested that the compositional diversity of Aluto pantellerites is consistent with fractional crystallisation of a 'rift-related' basalt. However, they did not explore the major element liquid line of descent, phase equilibria constraints, mineral compositions or the physical conditions under which magmas may have been stored. Here, we build on the work of Hutchison et al. (2016b), first characterising the petrology of Aluto pantellerites, then using whole-rock and mineral analyses to investigate the plausibility of magma genesis through closed-system fractional crystallisation and to determine the conditions of magma storage.

3   PETROLOGY.

Thin sections of representative basaltic and pantelleritic samples were analysed using an FEI Quanta FEG-scanning electron microscope to characterise mineral textures and identify compositional zoning. Phenocryst phase proportions in basaltic sample 17-01-05 were determined by Energy-Dispersive X-ray Spectrometry (EDS) mapping and subsequent phase analysis (Supplementary Material Table S.1 and Fig. S.1).

Original Manuscript

Major element compositions of olivine, alkali feldspar, and plagioclase feldspar phenocrysts were analysed using a Cameca SXFive FEG-electron microprobe (EPMA) at the Department of Earth Sciences, University of Oxford. Matrix glass compositions in pantelleritic samples were determined using a JEOL 8600 EPMA at the Research Laboratory for Archaeology and the History of Art, University of Oxford.

Mineral analyses were collected using a 15 kV, 10 nA, defocussed (10 μm spot) electron beam. All elements were counted on-peak for 30s with the exceptions of Na (12s; analysed first to avoid alkali-loss) and Mn, P and Ti (60s). Matrix glass analyses were collected using a 15 kV, 6 nA, defocussed (10 μm spot) electron beam, with SiO_2 and Na_2O analysed first to avoid potential alkali-loss during analysis (Humphreys et al., 2006). The count time on Mn was reduced to 50s on peak. For all elements in minerals and glasses, backgrounds were collected either side of the peak for half of the on-peak count time. Data quality was routinely monitored using secondary glass and/or mineral standards analysed at the start and end of each run. In general, the measured values of the secondary standards fall within 2σ of the published values (Jochum et al., 2006). Results from EPMA are reported in Supplementary Material A.1; A.2; A.3.

3.1 BASALTS

Sample 17-01-05 is a Quaternary rift-related basalt collected to the north-east of the main Aluto complex. It is porphyritic with the phenocryst assemblage: plagioclase feldspar + olivine + clinopyroxene + minor orthopyroxene. Magnetite is present in the microcrystalline groundmass. Olivine phenocrysts are typically 0.25-1 mm in diameter and are generally euhedral or subhedral. These olivine phenocrysts account for ~10% of the sample (Supplementary Table S.1) and are zoned, with narrow (~20-50 μm) Fe-rich rims (Fo_{66-80}) and more Mg-rich cores (Fo_{80-87}) (Supplementary Material A.3). EPMA analysis reveals that olivine cores have a uniform composition. The Mg-rich cores formed in a more primitive (Mg-rich) magma than the surrounding groundmass, which was

Original Manuscript

compositionally similar to the whole-rock composition of sample 17-01-05 (Supplementary Material Fig. S.2).

Clinopyroxene and plagioclase phenocrysts in sample 17-01-05 are unzoned and subhedral. The sample has a subophitic texture, indicating that clinopyroxene grew contemporaneously or after plagioclase crystallisation (Fig. 2). A few large (>1 mm diameter) clinopyroxene and plagioclase phenocrysts have Fe or Na-rich cores overgrown by Mg or Ca-rich rims (<300 μm wide), respectively.

3.2 PERALKALINE RHYOLITE

The pantellerite lavas are variably porphyritic (5-40% phenocrysts by volume), with the phase assemblage: alkali feldspar + quartz ± aenigmatite ± clinopyroxene ± apatite ± biotite ± Fe-Ti oxides (Fig. 3). All phenocryst phases are unzoned and do not show disequilibrium textures (e.g. sieve textures). Alkali feldspar and quartz have a granophyric texture, attesting to their co-precipitation (Fig. 2). Alkali feldspar compositions cover a restricted compositional range within individual samples (e.g. Or_{45} to Or_{49}), but vary from Or_{30} to Or_{49} between samples, crossing the divide between Anorthoclase and Sanidine (Supplementary Material A.1). Alkali feldspar phenocrysts that are not intergrown with quartz crystals in a granophyric texture are typically euhedral to subhedral, and form elongate crystals (up to 3mm long). Little to no chemical zonation is apparent in the alkali feldspar phenocrysts.

3.3 THERMOMETRY

Temperature estimates were obtained from EPMA analysis of the rim compositions of alkali feldspar phenocrysts and matrix glass from 6 pantellerite lava samples (Supplementary Material A.1; A.2), using the alkali-feldspar – melt geothermometer of Putirka (2008). These temperatures represent the crystallisation temperature of the alkali feldspar rims, and range from 718-765°C. A standard error of ±23°C is associated with this analysis (Putrika, 2008). We have assumed that the alkali feldspar rims are in equilibrium with the surrounding matrix glass. This is supported by the lack of disequilibrium textures or compositionally zoned rims in the alkali feldspar phenocrysts. Within a

Original Manuscript

particular sample, the maximum temperature variation observed is <30°C, and most vary by <15°C (Supplementary Fig S.4). This is in agreement with Rhyolite-MELTS models, which indicate that crystallisation of alkali-feldspar dominates the crystallising assemblage below a temperature of ~800°C (see sections 5 and 6).

4   THERMODYNAMIC MODELLING

Thermodynamic modelling of the compositional evolution of liquid and mineral phases in Aluto magmas was carried out using the Rhyolite-MELTS thermodynamic modelling software (Gualda et al., 2012). This model calculates the stable phase assemblage of a system under given conditions (e.g. P, T, fO_2) through a free-energy minimisation. Rhyolite-MELTS is calibrated from experimental datasets for fluid-bearing silicic systems (Gualda et al., 2012). It been used successfully to investigate magma storage conditions in metaluminous and peralkaline systems (e.g. Fowler et al. 2007; Fowler and Spera, 2010; Cannatelli, 2012; Pamukcu et al., 2015; Stock et al., 2016).

Here, we use Rhyolite-MELTS to investigate phase equilibria during crystallisation of primitive melts at Aluto. Pressure is held constant in our models (i.e. isobaric conditions); phase proportions and solid/liquid compositions are calculated as the temperature drops (starting at the liquidus), with crystal phases extracted from the bulk composition at each temperature step (i.e. fractional crystallisation). We ran simulations with 2°C temperature intervals as using larger temperature intervals would influence the resolution of the fractional crystallisation models. Pressure, initial H_2O concentration and fO_2 were varied systematically over a realistic range (50-300 MPa, 0.5-3 wt% and -2 – +1 log units below/above the Quartz-Fayalite-Magnetite [QFM] buffer, respectively), covering the range of potential magma storage conditions identified previously in peralkaline systems (Table 2). Model outputs are compared with empirical geochemical data to determine the 'best fit' parameters that represent the most likely magma storage conditions during pre-eruptive crystallisation at Aluto (section 4.2).

Original Manuscript

We test the sensitivity of our models to the choice of starting composition by using two distinct basalt samples as liquidus compositions, which represent different potential estimates of the Aluto parental melt. These samples represent the most primitive basalts measured in Aluto, as defined by their Mg number (Mg#=MgO/[FeO$_t$+MgO]). Sample DP4 is a mafic picrobasalt clast from a scoria cone near the Aluto caldera (Di Paola, 1972). Sample 17-01-05 is a basaltic scoria clast from a cone to the East of Aluto (Hutchison et al., 2016b). Sample 17-01-05 has significantly higher MgO and SiO$_2$ contents than DP4 (Table 1). One hundred and forty four fractional crystallisation models were run for each potential Aluto starting composition, covering the full range of P, H$_2$O, fO$_2$ conditions.

We assume that whole-rock compositions from Aluto are representative of magma (liquid) composition. Since the samples are generally phenocryst-poor, and measured matrix glass compositions are indistinguishable from whole rock in terms of their major element chemistry, this assumption is reasonable. The anhydrous component of the modelled compositions are normalised to 100% for comparison between empirical data and modelled compositions.

4.1   MODEL LIMITATIONS

Gualda et al. (2012) note that Rhyolite-MELTS does not accurately model the formation of hydrous phases such as amphibole. This influences the accuracy of Rhyolite-MELTS when modelling the evolution of intermediate magma compositions with high H$_2$O contents (Gualda et al., 2012). However, biotite and apatite are the only hydrous minerals present in Aluto and are volumetrically minor. Biotite generally accounts for <2% of the phenocryst assemblage (Fig. 3), and apatite only occurs as an accessory phase (<1%; Fig.3). Consequently, we expect that inaccuracies in modelling the stability of hydrous minerals will have a negligible effect on our model outputs.

Rooney et al. (2012) note that Rhyolite-MELTS consistently over-predicts magmatic P$_2$O$_5$ concentrations, due to inaccuracies in the apatite solubility model. However, as apatite is only a minor accessory phase, this is also unlikely to have a significant effect on the major element evolution of the melt in our models. Additionally, Fowler and Spera (2010) identified that Rhyolite-

Original Manuscript

MELTS often over predicted the CaO content of the empirically determined compositions of natural samples. This is attributed to the 'under-stabilisation' of clinopyroxene (Fowler and Spera, 2010), however, it does not seem to have a significant effect on the concentration of other major oxides in the melt.

Other potential limitations relate specifically to peralkaline systems. While multiple studies have used MELTS to investigate magmatic evolution in peralkaline volcanoes (Peccerillo et al., 2003; Ronga et al., 2009; Rooney et al., 2014), it is clear that some common peralkaline mineral phases (notably aenigmatite $[(Na,Ca)_4(Fe^{2+},Ti,Mg)_{12}Si_{12}O_{40}]$) are not accurately modelled. This is because there is insufficient experimental data on aenigmatite stability in peralkaline melts to accurately constrain its thermodynamic properties in Rhyolite-MELTS. Although aenigmatite is present in most obsidian samples from Aluto, it only occurs in minor modal quantities (Fig. 4), and is considered to be a late-crystallising phase, forming only at low temperatures, after a drop in melt Al_2O_3 following alkali feldspar precipitation (Neave et al., 2012). Consequently, inaccuracies in modelling aenigmatite should not influence the liquid line of descent until very late in fractional crystallisation, and thus does not significantly influence our results.

4.2 A STATISTICAL METHOD FOR IDENTIFICATION OF 'BEST FIT CONDITIONS' IN RHYOLITE-MELTS MODELS

Previous studies have determined magmatic crystallisation conditions by comparing Rhyolite-MELTS outputs run at different conditions with empirical datasets (e.g. Fowler et al., 2007; Fowler and Spera, 2010; Cannatelli, 2012). Typically, the 'best-fit' models are identified qualitatively by visual assessment. We have developed a statistical routine to quantify the fit between the modelled composition of the residual melt and the geochemical data. This approach is based on a least-squares analysis, where the sum of the squared residuals between the measured whole-rock data and modelled magma compositions is used to identify the model that most accurately reproduces the composition of natural samples. This method is explained in Table 3. The sum of the squared residuals is calculated from:

Original Manuscript

$$\sum_{X}^{m} \left(\frac{\sum_{i}^{n}(X_i - \hat{X})^2}{X_{SD}} \right)_X$$

(Eqn. 1)

where, n is the number of natural samples whose compositions represent the 'target' compositions for the fractional crystallisation models (i.e. the compositions that we are attempting to reproduce via fractional crystallisation); m is the number of oxides considered in the analysis; X_i is the concentration of oxide X determined by whole-rock analysis of sample i; $\hat{X}$ is the concentration of oxide X predicted by Rhyolite-MELTS at a particular temperature; X_{SD} is the standard deviation of oxide X in all the empirically determined compositions of natural samples representing the 'target' compositions. In all cases, elemental concentrations are in oxide wt%.

This analysis is carried out for every point in a single fractional crystallisation model (i.e. at every temperature step the composition generated by Rhyolite-MELTS is compared to the whole-rock data; Table 3). The temperature point with the lowest calculated residual is then used to represent how closely that model matches the composition of the natural samples (Table 3). We refer to this method as the minimum Weighted Squared Residual (mWSR) method. However, taking only one point of a Rhyolite-MELTS model to represent the 'fit' may give anomalous results (Fig. 4a). We therefore developed a second method, which averages the 15 lowest residuals for each model (referred to as the average Weighted Squared Residual method – aWSR). Using greater than 15 analyses tends to give erroneous results because some of our models terminate at a melt fraction of f~0.1 (after which Rhyolite-MELTS failed to converge), whereas others were able to progress to f<0.05 (explained in Fig. 4b).

The aWSR method provides a means to quickly and easily evaluate intrinsic variables of magma storage, and determine the models that most likely represent the conditions of natural magma storage. The strength of this method is not only that it is a statistically robust, quantitative determination of magma storage conditions from modelling data, but the speed and ease of

Original Manuscript

analysis. In previous studies (e.g. Fowler et al., 2007; Fowler and Spera, 2010; Cannatelli, 2012) predicted mineral abundances and compositions are also compared to those observed in natural samples. These factors are not included in the statistical routine described above, and are difficult to apply to Aluto, due to low crystallinity and the formation of certain phenocryst phases (e.g. aenigmatite) which are not accurately modelled by Rhyolite-MELTS.

5 RESULTS FROM RHYOLITE-MELTS MODELLING

5.1 STARTING COMPOSITION

Samples DP4 and 17-01-05 were used as parental magma compositions in the fractional crystallisation models. In general, models using 17-01-05 as the starting composition display a better match to the composition of the volcanic products from Aluto, which is confirmed by aWSR analysis (Supplementary Fig. S.3). DP4 models under predict K_2O and over predict the Na_2O content of the pantelleritic rhyolites, except at high fO_2 (>QFM+1). This is because, the DP4 starting composition contains more sodium than 17-01-05, and an increase in the K_2O content at constant SiO_2 is not seen due to the earlier formation of spinel in models using DP4 as the starting composition. Such high fO_2 conditions are not expected in peralkaline magmas (fO_2 is likely between QFM and QFM-1 in peralkaline magmas; Macdonald, 2012) and we therefore suggest that 17-01-05 represents a better approximation of the parental magma composition. Additionally, using sample 17-01-05 as a starting composition, Hutchison et al. (2016b) were able to successfully model the trace element variation during magmatic evolution at Aluto. The whole-rock composition of sample 17-01-05 is therefore taken as the best estimate of the Aluto parental magma. Future work to determine the composition of primitive mafic samples in the region would greatly aid future investigations of magmatic differentiation at peralkaline volcanic centres in the MER.

5.2 LIQUID LINE OF DESCENT

All models using 17-01-05 as a starting composition display similar geochemical trends as minerals are predicted to crystallise in a similar order and at similar temperatures (Fig. 5). Olivine is the first

Original Manuscript

mineral predicted to precipitate at the liquidus (1260-1213°C), causing a large decrease in the MgO content and a smaller increase in the SiO_2 concentration of the residual liquid over a short crystallisation interval (Fig. 5e). Clinopyroxene is the next phase to appear on the liquidus at only slightly lower temperatures (1185°C at fO_2 = QFM; P = 150 MPa; H_2O = 0.5 wt%; Fig. 6b). At this point, the liquid SiO_2 concentration begins to decrease along with CaO. The liquid MgO content continues to decrease markedly over a short crystallisation interval and the concentrations of other key oxides (Na_2O, K_2O, Al_2O_3 and TiO_2) increase slightly.

Spinel and plagioclase are the next minerals that are predicted to precipitate, but the order in which they come onto the liquidus depends on the magma storage conditions. Plagioclase will generally precipitate first, but at high fO_2 (QFM+1) and high initial H_2O contents (≥1 wt%) spinel precipitates first. At fO_2 = QFM; P = 150 MPa; initial H_2O = 0.5 wt%, plagioclase precipitates at 1159°C and spinel precipitates at 1117°C (Fig. 6b). However, at fO_2 = QFM+1; P = 150 MPa; initial H_2O = 1 wt%, plagioclase precipitates at 1116°C after spinel at 1134°C. Crystallisation of these minerals has a major influence on the composition of the residual liquid. Notably, when spinel starts to precipitate, the liquid SiO_2 concentration begins to increase significantly over a short crystallisation interval and the TiO_2 concentration decreases. Models predict that plagioclase feldspar is initially Ca-rich (An_{80}-An_{90}), causing a continual decrease in the liquid CaO content. Additionally, formation of plagioclase causes a decrease in the liquid Al_2O_3 concentration. After the *plagioclase-* and *spinel-in*, there is a reduction in the magnitude of decrease in MgO per unit crystallisation.

As fractional crystallisation continues, plagioclase, olivine, clinopyroxene and spinel dominate the mineral assemblage, leading to a continual decrease in MgO, FeO_t, Al_2O_3 and TiO_2 and an increase in the Na_2O, K_2O and SiO_2 contents of the residual liquid over a protracted temperature interval (i.e. 1150-900°C). The SiO_2 content of the residual liquid can be used as a fractionation index to measure the degree of differentiation (higher SiO_2 represents more differentiated melts).

Original Manuscript

As the residual liquid evolves towards more SiO_2-rich compositions, modelled feldspar compositions become more sodic. Consequently, the degree of Na_2O enrichment in the residual liquid per unit crystallisation decreases during magmatic evolution. Rhyolite-MELTS predicts sanidine crystallisation late in magmatic evolution (~90% crystallisation; Fig. 6). At this point, K_2O becomes compatible with the crystallising mineral assemblage and is significantly depleted in the residual liquid over a short crystallisation interval (Fig. 5b). Modelled sanidine compositions are more calcic than those measured in natural samples. This is likely due to known inaccuracies in the modelling of magmatic CaO evolution in Rhyolite-MELTS (Section 4.1; Fowler and Spera, 2010).

The FeO_t concentration of the residual melt predicted in Rhyolite-MELTS models at high SiO_2 (>70 wt%) does not match that observed in the pantellerites from Aluto (Fig 5h). This may be due to inaccuracies in modelling of aenigmatite stability in pantelleritic melts; Rhyolite-MELTS predicts crystallisation of Fayalite and Fe-Ti oxides instead of aenigmatite during magmatic differentiation. These minerals contain more Fe than aenigmatite, resulting in lower FeO_t values. As stated previously, aenigmatite is only likely to form very late during fractional crystallisation (following alkali feldspar formation when the magma becomes enriched in Na_2O relative to Al_2O_3; Neave et al., 2012) and is a relatively minor modal component. Therefore, inaccuracies in aenigmatite modelling only affect the model results at very low temperatures and do not have an important influence on the concentration of the major elements until very low melt fractions (f<0.05).

5.3 EFFECTS OF OXYGEN FUGACITY

The stability of spinel group minerals in Rhyolite-MELTS models is affected by changes in the system fO_2. At higher fO_2, the stability of spinel minerals increases in the melt, and they precipitate at higher temperatures. Consequently, the increase in magmatic SiO_2 concentration that accompanies *spinel-in* begins at higher temperatures. Enhanced spinel crystallisation at elevated fO_2, causes lower Na_2O and higher MgO concentrations in the residual melt at a given SiO_2 concentration (Fig. 7). At low fO_2 (QFM-2), *plagioclase-in* can occur up to 80^oC before spinel crystallisation, causing a reduction in the

Original Manuscript

Al_2O_3 content of the magma during the early stages of differentiation. At higher fO_2, plagioclase forms alongside or after spinel. As a result, the Al_2O_3 concentration of the residual melt does not decrease prior to an increase in the SiO_2 concentration caused by spinel fractionation, resulting in a higher Al_2O_3 concentration at similar SiO_2 content in models at higher fO_2.

Earlier formation of spinel group minerals explains the smaller increase of TiO_2 during magmatic cooling in models at fO_2 = QFM+1, relative to models at fO_2 = QFM-2 – QFM. Additionally, variability in fO_2 influences the composition of spinel group minerals. At fO_2= QFM+1, spinel minerals contain less TiO_2 than at lower fO_2. Therefore, at fO_2 = QFM-2 – QFM there is greater reduction of TiO_2 after *spinel-in*.

Overall, models at fO_2 = QFM – QFM+1 provide a better match to the geochemical data of eruptive products from Aluto than those at fO_2<QFM. Models at low fO_2 (QFM-2 – QFM-1) under predict the Al_2O_3 and TiO_2 contents of the pantelleritic rhyolites at Aluto, and over predict the K_2O and Na_2O contents.

5.4 PRESSURE

At pressures >200 MPa, leucite is predicted as a stable mineral phase in Rhyolite-MELTS models. As leucite is not present in any Aluto samples, isobaric fractional crystallisation at >200 MPa is considered implausible. At lower pressures, variability in the modelled liquid line of descent is largely the result of variable feldspar stability. Plagioclase stability is inversely correlated with pressure, causing an increase in Al_2O_3 and a decrease in the MgO content of the melt at a given SiO_2 concentration in higher pressure models (Fig. 8). Conversely, as pressure increases the stability of sanidine increases, in agreement with previous work (Blundy and Cashman, 2001). Earlier sanidine crystallisation at elevated pressures causes K_2O and Al_2O_3 to decrease in the melt at higher temperatures (and SiO_2 concentrations) as crystallisation progresses. At pressures of ~200 MPa, Rhyolite-MELTS predicts formation of an Al- and Ti-rich clinopyroxene causing a decrease in the MgO, Al_2O_3 and TiO_2 contents of the residual liquid. Models at lower pressures (50 MPa) slightly over

Original Manuscript

predict the MgO and under predict the K_2O content of the natural pantelleritic samples. Therefore the composition of the natural samples from Aluto are best reproduced by models at 100 - 150 MPa.

5.5   INITIAL WATER CONTENT

Higher initial H_2O contents reduce plagioclase stability, resulting in magmas with higher Al_2O_3 and lower MgO contents than those with lower initial H_2O at equivalent SiO_2 concentrations. Furthermore, higher initial H_2O content (>1 wt%) induces crystallisation of a second high Ti-clinopyroxene phase, in addition to the relatively Ti-poor clinopyroxene that is seen in all other models. This causes a decrease in the TiO_2 content of the melt at a given temperature, relative to lower H_2O models. As a result, models with lower initial H_2O contents (0.5 wt%) best reproduce the composition of the basaltic and intermediate samples from Aluto (Fig 9).

When fO_2 = QFM and P = 100 MPa, the composition of the pantelleritic rhyolites from Aluto can be reproduced reasonably well, regardless of the initial H_2O content. However, low H_2O content (0.5 wt%) models at higher pressures (~150 MPa) are able to more accurately reproduce the composition of these samples. In models with initial H_2O contents ≥1 wt%, the Na_2O content of the melt is under predicted at pressures >100 MPa, due to increased stability of more albitic plagioclase. At low initial H_2O contents (0.5 wt%), changing the crystallisation pressure only has a minor effect on the liquid line of descent, but using our statistical approach, it is possible to determine that magma is most likely stored at 150 MPa (Section 5.6).

5.6   STATISTICAL RESULTS AND SUMMARY OF 'BEST FIT' MAGMA STORAGE CONDITIONS AT ALUTO

The aWSR analysis quantitatively verifies the magma storage conditions at Aluto, which best reproduce the compositions of natural samples (Fig. 10). This builds on previous studies (e.g. Fowler et al. 2007; Cannatelli, 2012), which identified these 'best fit' conditions qualitatively. The results reveal that models at fO_2 < QFM have a very poor match to the composition of pantelleritic rhyolites at Aluto. The 'best fit' models are consistently at fO_2 = QFM, with models at fO_2 = QFM+1 producing

Original Manuscript

marginally higher residuals (Fig 10a). At a given fO_2 and initial H_2O content, the lowest residuals are produced in models at P = 100 – 150 MPa, depending on the initial H_2O content (Fig 10b). However, the lowest residual, and hence the best match to the compositional data of pantellerites from Aluto, is at 0.5 wt% initial H_2O and P = 150 MPa. At these low H_2O contents, pressure does not influence the results as much as it does at higher H_2O contents. At initial H_2O contents >1 wt%, models at P > 100 MPa produce a very poor fit to the compositional data from Aluto (Fig 10c). Higher residuals are consistently produced in models at P = 50 MPa, compared to those at 100 and 150 MPa. In summary, the Rhyolite-MELTS models that best reproduce the natural composition of Aluto whole-rock samples were run at fO_2 = QFM; P = 150 MPa; initial H_2O = 0.5 wt%.

6 DISCUSSION

6.1 MAGMA STORAGE CONDITIONS

We have shown that the composition of the pantellerite lavas from Aluto can be generated by protracted fractional crystallisation without the need for crustal assimilation. Around 90% fractional crystallisation is required to produce these compositions, in agreement with previous trace element and isotopic studies (Hutchison et al., 2016b). This represents a similar degree of fractional crystallisation to that required for rhyolite genesis at other peralkaline volcanic centres (Peccerillo et al., 2003; White et al., 2009). This extensive crystallisation indicates that the Aluto magma reservoir is likely exists as a highly crystalline magmatic mush from which viscous silicic magmas are extracted prior on eruption. This is supported by magnetotelluric data, which shows no evidence for a low-resistivity melt zone at the shallow crustal levels determined for magma storage in this study (Samrock et al., 2015). Such mush chambers are commonly inferred to exist beneath rhyolitic volcanoes (Bachmann and Bergantz, 2008).

Our aWSR analysis indicates that Aluto magma crystallises with fO_2 around the QFM buffer (Fig. 10a). This is supported by the presence of Ti-bearing aenigmatite, which is stable at fO_2 between the QFM and Nickel-Nickel Oxide buffers and a pressure of ~100 MPa (Scaillet and Macdonald, 2001;

Original Manuscript

Ronga et al., 2009). Crystallisation at fO_2 = QFM is consistent with other peralkaline systems (Macdonald, 2012).

The statistical results show that models with initially low H_2O contents (0.5 wt%) generally have a better match to the pantelleritic rhyolites from Aluto than models run with higher starting H_2O contents (Fig 10c). Additionally, low initial H_2O contents (0.5 wt%) produce a better match to the basaltic and intermediate products at Aluto (Fig. 9). These low H_2O contents in Aluto parental magmas are consistent with results from previous studies on peralkaline volcanism in the MER and elsewhere (section 6.3). Low H_2O contents increase plagioclase stability in the magma, resulting in a greater reduction of Al_2O_3 due to plagioclase crystallisation and increasing the peralkalinity of the residual melt.

The predicted low initial H_2O content of Aluto melts implies that volatile saturation is only expected to occur at low pressures or after significant crystallisation (~90-95% crystallisation, similar to the amount of crystallisation required to produce the composition of pantellerites from Aluto; Fig. 6b). This may play an important role in 'priming' the system for eruption (e.g., Stock et al., 2016); late-stage exsolution of a magmatic vapour phase would increase the overpressure of the magma chamber (Tait et al., 1989; Fowler and Spera, 2008) and the buoyancy of the magma (Degruyter and Huber, 2014). Hence, volatile saturation may increase the 'eruptibility' of highly silicic pantelleritic magmas.

Destabilisation of crystalline mush by injection of hotter, more mafic magma into the system has been suggested as a potential eruption triggering mechanism in many studies (e.g. Murphy et al., 2000; Christopher et al., 2010). However, instability of the crystalline mush may also occur due to large contrasts in buoyancy between magma layers and the surrounding mush (Christopher et al., 2015). This mechanism for mush instability leading to eruption is consistent with the data presented here (i.e. volatile saturation occurs at a high degree of crystallisation and at a similar magmatic composition to the composition of the eruptive products), and the lack of petrographic or

Original Manuscript

geochemical evidence for magma mixing in the pantellerite samples from Aluto. In this regard Aluto differs from many other peralkaline volcanic centres (e.g. Boset; Ronga et al., 2009 and Dabbahu; Field et al., 2012), which show evidence for magma mixing of rhyolites with more mafic magmas. This may indicate more complex magmatic systems at these volcanic centres (i.e. multiple regions of magma storage).

At low H_2O contents (0.5 wt%) pressure variations only play a minor role in determining the liquid line of descent. However, our statistical analysis shows that the best match to the compositional data is at ~150 MPa (section 5.6). These relatively low pressures are supported by the presence of granophyric textures in rhyolitic magmas (Fig. 2), which are indicative of crystallisation at shallow depths (~3 km) where undercooling can occur due to volatile exsolution during magma ascent (Lowenstern et al., 1997). Additionally, independent experimental studies on peralkaline magmas have shown that the phase assemblage of alkali feldspar + clinopyroxene + aenigmatite + ilmenite is stable at 680-725°C and 100-150 MPa at near H_2O saturated conditions (Di Carlo et al., 2010). These experiments agree with our modelling results, except that the temperature range is slightly below the estimated eruptive temperatures for our pantellerite samples (section 3.3).

The stratigraphy beneath Aluto is well-constrained by 8 exploratory geothermal wells, the deepest of which reaches 2500 m depth (Gianelli and Teklemariam, 1993; Gizaw, 1993; Teklemariam et al., 1996; Hutchison et al., 2015). The uppermost section is dominated by recent silicic lava and pumice deposits, which are underlain by lacustrine and ignimbrite deposits in the next ~400 m. These are underlain by a sequence of predominantly mafic lavas (informally known as the Bofa Basalts), which range from 800-1000 m in thickness. At the base of the sequence is the >700 m thick, highly vesicular, Neogene ignimbrite (the base of this unit has not been identified; Teklemariam et al., 1996; Hutchison et al., 2015). Using this stratigraphy and average rhyolite, sedimentary, and basalt deposits densities of 2500 kg/m^3, 2500 kg/m^{3}and 2900 kg/m^3 (DeNosaquo et al., 2009), respectively, gives an average crustal density of ~2625 kg/m^3 up to 2.5 km beneath Aluto (~65 MPa). At greater

Original Manuscript

depths, regional gravity surveys reveal that the crustal density beneath MER volcanoes (i.e. Boset) ranges from 2770-3000 kg/m^3 (Cornwell et al., 2006). Assuming an average crustal density of 2800 kg/m^3 at depths >2.5 km, the depth of magma storage at Aluto (i.e. crystallisation at 150 MPa) is ~5.6 ± 1 km (where errors represent uncertainty in the crustal density).

Previous studies have suggested the importance of polybaric crystallisation during magmatic differentiation in MER peralkaline volcanoes (Rooney et al., 2012; 2014). Our models demonstrate that complex plumbing systems, with crystallisation at different crustal levels are not necessary to generate the composition of Aluto samples and that these can be formed by isobaric crystallisation. Additionally, there is little or no evidence for magma mixing at Aluto from the petrological data, indicating that multiple magma storage regions are not required. This difference may be because previous work has investigated large-scale mush zones that generated major caldera-forming eruptions (e.g. Rooney et al., 2012), whereas, we have focused on smaller volume, post-caldera eruptive episodes. Variations in the incompatible trace element compositions at Aluto since ~60 ka can be explained by crystal fractionation in a compositionally zoned cap of a shallow magmatic reservoir (Macdonald et al., 2014; Hutchison et al., 2016b). Larger volume caldera forming eruptions are likely to be sourced from a larger chamber over a greater depth interval, polybaric models are therefore more relevant to these larger eruptions. Additionally, as little is currently known about magma storage conditions at Aluto, we have used the simplest approach, with fewest assumptions, in order to robustly determine the most likely magma storage conditions.

Mineral-melt equilibria using rim compositions from the alkali feldspar phenocrysts provides magmatic temperature estimates shortly before eruption. In Aluto, these mineral-melt equilibria reveal a relatively narrow temperature range between 718-765 ^{o}C (section 3.3). This is a much smaller eruptive temperature range than that observed in peralkaline rhyolites erupted from other peralkaline silicic centres (e.g. Pantelleria; White et al., 2009; Dabbahu, Field et al., 2012). This potentially reflects the restricted compositional diversity of Aluto products from the last ~60 ka,

Original Manuscript

relative to the compositional range of Dabbahu and Pantelleria eruptive products in the same age range (White et al., 2009; Field et al. 2012; 2013). Additionally, Dabbahu volcano displays several key differences to Aluto. Importantly, magma mixing has been shown to be an important process at Dabbahu, and magma is believed to be stored in a series of stacked sills, rather than a compositionally zoned magma reservoir (Field et al., 2012; 2013).

6.2 COMPARISON WITH RECENT ACTIVITY

6.2.1 Ground Deformation

Using a Mogi point source model, observed ground deformation in 2008 (i.e. inflation of ~10cm) is best explained by a deformation source at ~5.1 ± 0.5km depth (Hutchison et al., 2016a). This provides a better match to the observed horizontal displacement than an earlier model (Biggs et al., 2011), which proposed a shallow (2.5 km depth) penny shaped crack as the deformation source (see Hutchison et al., 2016a for discussion). C-isotope analysis of degassing CO_2 from Aluto suggests that the current ground deformation is, at least in part, the result of magmatic activity rather than hydrothermal fluids (Hutchison et al., 2016a). The 5.1 km deformation source is thought to represent the roof of a magmatic storage region (Hutchinson et al., 2016a) and is in good agreement with our petrological modelling results (Fig. 11).

6.2.2 Seismic Observations

Between January 2012 and January 2014, a network of seismometers was installed in the Aluto region (Wilks, 2016). A decrease in the number of seismic events recorded from 4 – 7 km depth directly beneath the Aluto caldera was identified (Wilks, 2016), corresponding with our predicted depth of magma storage before past eruptions. The decrease in seismicity in this region may be related to elevated temperatures close to a magma body, which would decrease the likelihood of brittle failure, resulting in a drop in seismicity. Therefore, the seismic evidence is consistent with the results of this study (Fig. 11).

Original Manuscript

6.3 COMPARISON TO OTHER MER VOLCANIC CENTRES

Boset and Gedemsa, two peralkaline silicic centres in the Northern MER, have been the subject of previous petrological and geochemical studies (Peccerillo et al., 2003; Ronga et al., 2009). These volcanoes have phase assemblages and peralkaline magmatic compositions that are similar to those seen at Aluto and MELTS modelling has been used to evaluate magmatic storage conditions at these locations (Peccerillo et al., 2003; Ronga et al., 2009). These studies indicate that storage conditions at Boset and Gedemsa are similar to those identified at Aluto (P = 50-100 MPa; fO_2 = QFM; H_2O = 1 wt%). We have compiled data on magmatic storage conditions from a number of other peralkaline volcanoes in the MER and elsewhere in Table 4. Although slight differences in the magmatic storage conditions can be identified between the different systems, this compilation indicates that peralkaline magmas, as hypothesised previously (Peccerillo et al., 2003; Caricchi et al., 2006; White et al., 2009) tend to be frequently generated by magmatic differentiation in the shallow crust (commonly <200 MPa) from parental melts with relatively low initial H_2O contents (typically ≤1 wt%) and at an oxygen fugacity close to the QFM buffer.

Regional gravity surveys in the MER reveal the presence of positive gravity anomalies within the shallow crust (Mahatsente et al., 1999; Cornwell et al., 2006). These are interpreted to represent crystallised magmatic intrusions, which often occur at depths of <4km (Mahatsente et al., 1999). These separate lines of evidence indicate that shallow magmatic storage systems are likely to be a common feature of many peralkaline silicic centres along the MER and suggest that silicic volcanism at MER volcanic centres is commonly fed by mafic intrusion and subsequent crystal fractionation in the shallow crust.

6.4 FORMATION OF A DALY GAP

There is a notable absence of intermediate magma compositions erupted at Aluto, which are predicted to form as a result of protracted fractional crystallisation from basaltic compositions to evolved pantellerites. This 'Daly Gap' is observed on a regional scale across the MER, and may relate to density stratification of magma reservoirs (Peccerillo et al., 2003; Ronga et al., 2009; Rooney et

Original Manuscript

al., 2012) whereby low-density silicic magmas occupy the shallower parts of any magmatic reservoir, and inhibit the eruption of higher density intermediate and basaltic compositions at the central volcanic centre (Peccerillo et al., 2003; Neave et al., 2012). At Aluto, a similar scenario, where recent pantelleritic eruptions are sourced from the top of a compositionally zoned chamber directly beneath the caldera, may exist and could explain why eruption of basaltic and intermediate composition lavas are restricted to a small number of volcanic cones to the NW of the main complex (Hutchison et al., 2016b). However, at Aluto, our thermodynamic modelling shows that SiO_2 does not change linearly with decreasing temperature. SiO_2 increases from 50 to ~64 wt% over a very short crystallisation interval, mainly due to the crystallisation of SiO_2-poor phases such as spinel (White et al., 2009), potentially causing the system to evolve rapidly through intermediate compositions (Figure 12). This has been proposed previously as a mechanism for generating a Daly Gap (Mushkin et al. 2002), including in other pantelleritic systems (White et al., 2009). As magma storage conditions for peralkaline systems tend to be very similar (section 6.3), we may expect the crystallising assemblage to be similar for many peralkaline systems. Therefore, it may not be surprising that many peralkaline volcanoes display a Daly Gap (Macdonald, 2012). The formation of the Daly Gap at Aluto is likely to be due to a combination of multiple factors including density stratification of a zoned magma reservoir beneath the Aluto caldera and the scarcity of intermediate composition magmas produced by the fractionation process.

7 CONCLUSIONS

1. Magma storage conditions can be evaluated using Rhyolite-MELTS to determine the simplest scenario (i.e. the scenario with the least number of assumptions) under which magmatic differentiation can produce the composition range of the eruptive products. We have developed a statistical routine that allows quantitative analysis of different parameters to identify the model (i.e. the set of parameters) that most closely predicts the compositions of

Original Manuscript

natural erupted products. This approach could be easily applied in other volcanic systems to identify the 'best fit' storage conditions.

2. We have constrained the pre-eruptive magma storage conditions of peralkaline rhyolites at Aluto by comparing modelled liquid lines of descent at different pressure, initial H_2O concentration and fO_2 (Rhyolite-MELTS) with the compositions of the eruptive products. Our results suggest that the erupted products most likely formed by fractional crystallisation of a parental basaltic magma with low initial H_2O content (0.5 wt%) and an fO_2 near the QFM buffer, at depths of ~5.6 ± 1 km (150 MPa). These results are consistent with pantelleritic phase equilibria experiments (Scaillet and Macdonald, 2001; Di Carlo et al., 2010), and textural evidence (e.g. granophyric texture; Lowenstern et al., 1997), and are in excellent agreement with the depth of the current melt zone beneath Aluto, interpreted from InSAR observations and seismic data.

3. Modelling isobaric fractional crystallisation using Rhyolite-MELTS reveals that Aluto pantellerite magmas can be generated by ~90% fractional crystallisation of a parental melt represented by basaltic sample 17-01-05, a rift-related basalt collected to the east of the main Aluto complex (Table 1). These models also reveal that assimilation of crustal material and/or polybaric processes are not required to produce the composition of the pantellerite samples from Aluto. The high degree of crystallisation required to generate these compositions suggests that the magma reservoir is likely to occur as a highly crystalline mush. This interpretation is supported by magnetotelluric data (Samrock et al., 2015).

4. The formation of the Daly Gap at Aluto is likely due to a combination of factors including density stratification and compositional zonation of the magma reservoir beneath the main caldera, and the scarcity of intermediate products produced during fractional crystallisation as SiO_2 increases from 50 to ~64 wt% over a very short crystallisation interval, mainly due to the crystallisation of SiO_2-poor phases such as spinel.

Original Manuscript

5. Comparison with other volcanic systems along the MER (e.g. Boset and Gedemsa) and in other tectonic settings (e.g. Pantelleria), and experimental data, indicate that magmatic storage in the upper crust is characteristic of many peralkaline systems. Additionally, low initial H_2O contents (≤1 wt%) and fO_2 near the QFM buffer appear to be characteristic storage conditions for peralkaline magmas globally.

ACKNOWLEDGEMENTS

REFERENCES

Abebe, B., Acocella, V., Korme, T. and Ayalew, D., 2007. Quaternary faulting and volcanism in the Main Ethiopian Rift. *Journal of African Earth Sciences*, *48*(2), pp.115-124.

Abebe, T., Manetti, P., Bonini, M., Corti, G., Innocenti, F., Mazzarini, F. and Pecskay, Z., 2005. Geological map (scale 1: 200,000) of the northern main Ethiopian rift and its implication for the volcano-tectonic evolution of the rift: Boulder. Colorado, Geological Society of America, Maps and Charts series, MCH094.

Agostini, A., Bonini, M., Corti, G., Sani, F. and Mazzarini, F., 2011. Fault architecture in the Main Ethiopian Rift and comparison with experimental models: Implications for rift evolution and Nubia–Somalia kinematics. *Earth and Planetary Science Letters*, *301*(3), pp.479-492.

Bachmann, O. and Bergantz, G.W., 2008. Rhyolites and their source mushes across tectonic settings. *Journal of Petrology*, *49*(12), pp. 2277-2285. DOI: 10.1093/petrology/egn068

Bohrson, W.A. and Reid, M.R., 1997. Genesis of silicic peralkaline volcanic rocks in an ocean island setting by crustal melting and open-system processes: Socorro Island, Mexico. *Journal of Petrology*, *38*(9), pp. 1137-1166. DOI: 10.1093/petroj/38.9.1137

Biggs, J., Bastow, I.D., Keir, D. and Lewi, E., 2011. Pulses of deformation reveal frequently recurring shallow magmatic activity beneath the Main Ethiopian Rift. *Geochemistry, Geophysics, Geosystems*, 12(9). DOI: 10.1029/2011GC003662

Black, S., Macdonald, R. and Kelly, M.R., 1997. Crustal origin for peralkaline rhyolites from Kenya: evidence from U-series disequilibria and Th-isotopes. *Journal of Petrology*, *38*(2), pp.277-297.

Original Manuscript

Blundy, J. and Cashman, K., 2001. Ascent-driven crystallisation of dacite magmas at Mount St Helens, 1980–1986. *Contributions to Mineralogy and Petrology*, *140*(6), pp.631-650. DOI: 10.1007/s004100000219

Cannatelli, C., 2012. Understanding magma evolution at Campi Flegrei (Campania, Italy) volcanic complex using melt inclusions and phase equilibria. *Mineralogy and Petrology*, 104(1-2), pp. 29-42. DOI: 10.1007/s00710-011-0182-6

Caricchi, L., Ulmer, P. and Peccerillo, A., 2006. A high-pressure experimental study on the evolution of the silicic magmatism of the Main Ethiopian Rift. *Lithos*, 91(1), pp. 46-58. DOI: 10.1016/j.lithos.2006.03.008

Cornwell, D.G., Mackenzie, G.D., England, R.W., Maguire, P.K.H., Asfaw, L.M. and Oluma, B., 2006. Northern Main Ethiopian Rift crustal structure from new high-precision gravity data. *Geological Society, London, Special Publications*, 259(1), pp. 307-321. DOI: 10.1144/GSL.SP.2006.259.01.23

Corti, G., 2009. Continental rift evolution: from rift initiation to incipient break-up in the Main Ethiopian Rift, East Africa. *Earth-Science Reviews*, 96(1), pp. 1-53. DOI: 10.1016/j.earscirev.2009.06.005

Corti, G., Sani, F., Philippon, M., Sokoutis, D., Willingshofer, E. and Molin, P., 2013. Quaternary volcano-tectonic activity in the Soddo region, western margin of the Southern Main Ethiopian Rift. *Tectonics*, *32*(4), pp.861-879. DOI: 10.1002/tect.20052

Christopher, T., Blundy, J., Cashman, K., Cole, P., Edmonds, M., Smith, P.J., Sparks, R.S.J. and Stinton, A., 2015. Crustal-scale degassing due to magma system destabilization and magma-gas decoupling at Soufrière Hills Volcano, Montserrat. *Geochemistry, Geophysics, Geosystems*, *16*(9), pp. 2797-2811. DOI: 10.1002/2015GC005791

Christopher, T., Edmonds, M., Humphreys, M. and Herd, R.A., 2010. Volcanic gas emissions from Soufrière Hills Volcano, Montserrat 1995–2009, with implications for mafic magma supply and degassing. *Geophysical Research Letters*, *37*(19). DOI: 10.1029/2009GL041325

Davies, G.R. and Macdonald, R., 1987. Crustal influences in the petrogenesis of the Naivasha Basalt—Comendite Complex: combined trace element and Sr-Nd-Pb isotope constraints. *Journal of Petrology*, *28*(6), pp.1009-1031.

Degruyter, W. and Huber, C., 2014. A model for eruption frequency of upper crustal silicic magma chambers. *Earth and Planetary Science Letters*, *403*, pp.117-130. DOI: 10.1016/j.epsl.2014.06.047

DeNosaquo, K.R., Smith, R.B. and Lowry, A.R., 2009. Density and lithospheric strength models of the Yellowstone–Snake River Plain volcanic system from gravity and heat flow data. *Journal of Volcanology and Geothermal Research*, *188*(1), pp.108-127. DOI: 10.1016/j.jvolgeores.2009.08.006

Di Carlo, I., Rotolo, S.G., Scaillet, B., Buccheri, V. and Pichavant, M., 2010. Phase equilibrium constraints on pre-eruptive conditions of recent felsic explosive volcanism at Pantelleria Island, Italy. *Journal of Petrology*, *51*(11), pp.2245-2276. DOI: 10.1093/petrology/egq055

Di Paola, G.M., 1972. The Ethiopian Rift Valley (between 7 00′ and 8 40′ lat. north). *Bulletin Volcanologique*, 36(4), pp. 517-560. DOI: 10.1007/BF02599823

Ebinger, C., 2005. Continental break-up: the East African perspective. *Astronomy & Geophysics*, *46*(2), pp.2-16. DOI: 10.1111/j.1468-4004.2005.46216.x

Original Manuscript

Ebinger, C., Ayele, A., Keir, D., Rowland, J., Yirgu, G., Wright, T., Belachew, M. and Hamling, I., 2010. Length and timescales of rift faulting and magma intrusion: The Afar rifting cycle from 2005 to present. *Annual Review of Earth and Planetary Sciences*, *38*, pp.439-466. DOI: 10.1146/annurev-earth-040809-152333

Ebinger, C.J. and Casey, M., 2001. Continental breakup in magmatic provinces: An Ethiopian example. *Geology*, 29(6), pp. 527-530. 67

Ferguson, D.J., Maclennan, J., Bastow, I.D., Pyle, D.M., Jones, S.M., Keir, D., Blundy, J.D., Plank, T. and Yirgu, G., 2013. Melting during late-stage rifting in Afar is hot and deep. *Nature*, 499(7456), pp. 70-73. DOI: 10.1038/nature12292

Field, L., Blundy, J., Brooker, R.A., Wright, T. and Yirgu, G., 2012. Magma storage conditions beneath Dabbahu Volcano (Ethiopia) constrained by petrology, seismicity and satellite geodesy. *Bulletin of Volcanology*, 74(5), pp. 981-1004. DOI: 10.1007/s00445-012-0580-6

Field, L., Blundy, J., Calvert, A. and Yirgu, G., 2013. Magmatic history of Dabbahu, a composite volcano in the Afar Rift, Ethiopia. *Geological Society of America Bulletin*, *125*(1-2), pp.128-147. DOI: 10.1130/B30560.1

Fontijn, K., Elburg, M.A., Nikogosian, I.K., van Bergen, M.J. and Ernst, G.G., 2013. Petrology and geochemistry of Late Holocene felsic magmas from Rungwe volcano (Tanzania), with implications for trachytic Rungwe Pumice eruption dynamics. *Lithos*, 177, pp. 34-53. DOI: 10.1016/j.lithos.2013.05.012

Fowler, S.J., Spera, F.J., Bohrson, W.A., Belkin, H.E. and De Vivo, B., 2007. Phase equilibria constraints on the chemical and physical evolution of the Campanian Ignimbrite. *Journal of Petrology*, 48(3), pp. 459-493. DOI: 10.1093/petrology/egl068

Fowler, S.J. and Spera, F.J., 2008. Phase equilibria trigger for explosive volcanic eruptions. *Geophysical Research Letters*, *35*(8). DOI: 10.1029/2008GL033665

Fowler, S.J. and Spera, F.J., 2010. A metamodel for crustal magmatism: phase equilibria of giant ignimbrites. *Journal of Petrology*, *51*(9), pp.1783-1830. DOI: 10.1093/petrology/egq039

Gianelli, G. and Teklemariam, M., 1993. Water-rock interaction processes in the Aluto-Langano geothermal field (Ethiopia). *Journal of volcanology and geothermal research*, 56(4), pp. 429-445. DOI: 10.1016/0377-0273(93)90007-E

Giordano, F., D'Antonio, M., Civetta, L., Tonarini, S., Orsi, G., Ayalew, D., Yirgu, G., Dell'Erba, F., Di Vito, M.A. and Isaia, R., 2014. Genesis and evolution of mafic and felsic magmas at Quaternary volcanoes within the Main Ethiopian Rift: Insights from Gedemsa and Fanta'Ale complexes. *Lithos*, 188, pp. 130-144. DOI: 10.1016/j.lithos.2013.08.008

Gizaw, B., 1993. Aluto-Langano geothermal field, Ethiopian Rift Valley: physical characteristics and the effects of gas on well performance. *Geothermics*, *22*(2), pp.101-116. DOI: 10.1016/0375-6505(93)90050-W

Gualda, G.A., Ghiorso, M.S., Lemons, R.V. and Carley, T.L., 2012. Rhyolite-MELTS: a modified calibration of MELTS optimized for silica-rich, fluid-bearing magmatic systems. *Journal of Petrology*, 53(5), pp. 875-890. DOI: 10.1093/petrology/egr080

Original Manuscript

Humphreys, M., Kearns, S.L. and Blundy, J.D., 2006. SIMS investigation of electron-beam damage to hydrous, rhyolitic glasses: Implications for melt inclusion analysis. *American Mineralogist*, *91*(4), pp.667-679. DOI: 10.2138/am.2006.1936

Hutchison, W., Biggs, J., Mather, T. A., Pyle D. M., Lewi, E., Yirgu, G., Caliro, S., Chiodini, G., Clor, L. E., and Fischer, T., 2016a. Causes of unrest at silicic calderas in the East African Rift: new constraints from InSAR and soil-gas chemistry at Aluto volcano, Ethiopia. *Geochemistry, Geophysics, Geosystems* 17, pp3008-3030. DOI: 10.1002/2016GC006395

Hutchison, W., Fusillo, R., Pyle, D.M., Mather, T.A., Blundy, J.D., Biggs, J., Yirgu, G., Cohen, B.E., Brooker, R.A., Barfod, D.N. and Calvert, A.T., 2016c. A pulse of mid-Pleistocene rift volcanism in Ethiopia at the dawn of modern humans. *Nature Communications*, *7*, 13192. DOI: 10.1038/ncomms13192.

Hutchison, W., Mather, T.A., Pyle, D.M., Biggs, J. and Yirgu, G., 2015. Structural controls on fluid pathways in an active rift system: A case study of the Aluto volcanic complex. *Geosphere*, 11(3), pp. 542-562. DOI: 10.1130/GES01119.1

Hutchison, W., Pyle D. M., Mather, T. A., Yirgu, G., Biggs, J., Cohen, B. E., Barford, D. N., and Lewi, E. 2016b. The eruptive history and magmatic evolution of Aluto volcano: new insights into silicic peralkaline volcanism in the Ethiopian rift. *Journal of Volcanology and Geothermal Research*. DOI: 10.1016/j.jvolgeores.2016.09.010

Jeffery, A.J., Gertisser, R., O'Driscoll, B., Pacheco, J.M., Whitley, S., Pimentel, A. and Self, S., 2016. Temporal evolution of a post-caldera, mildly peralkaline magmatic system: Furnas volcano, São Miguel, Azores. *Contributions to Mineralogy and Petrology*, *171*(5), pp.1-24.

Jochum, K.P., Stoll, B., Herwig, K., Willbold, M., Hofmann, A.W., Amini, M., Aarburg, S., Abouchami, W., Hellebrand, E., Mocek, B., Raczek, I., Stracke, A., Alard, O., Bouman, C., Becker, S., Dücking, M., Bratz, H., Klemd, R., de Bruin, D., € Canil, D., Cornell, D., de Hoog, C.-J., Dalpe, C., Danyushevsky, L., Eisenhauer, A., Gao, Y., Snow, J.E., Groschopf, N., Günther, D., Latkoczy, C., Guillong, M., Hauri, E.H., Hofer, H.E., Lahaye, Y., Horz, K., Jacob, D.E., Kasemann, S.A., € Kent, A.J.R., Ludwig, T., Zack, T., Mason, P.R.D., Meixner, A., Rosner, M., Misawa, K., Nash, B.P., Pf€ ander, J., Premo, W.R., Sun, W.D., Tiepolo, M., Vannucci, R., Vennemann, T., Wayne, D., Woodhead, J.D., 2006. MPI-DING reference glasses for in situ microanalysis: new reference values for element concentrations and isotope ratios. *Geochemistry, Geophysics, Geosystem*. 7, Q02008. DOI: 10.1029/2005GC001060

Kebede, S., 2012. Geothermal exploration and development in Ethiopia: status and future plan.

Keir, D., Bastow, I.D., Corti, G., Mazzarini, F. and Rooney, T.O., 2015. The origin of along-rift variations in faulting and magmatism in the Ethiopian Rift. *Tectonics*, *34*(3), pp.464-477. DOI: 10.1002/2014TC003698

Keir, D., Hamling, I.J., Ayele, A., Calais, E., Ebinger, C., Wright, T.J., Jacques, E., Mohamed, K., Hammond, J.O., Belachew, M. and Baker, E., 2009. Evidence for focused magmatic accretion at segment centers from lateral dike injections captured beneath the Red Sea rift in Afar. *Geology*, 37(1), pp. 59-62. DOI: 10.1130/G25147A.1

LeMasurier, W.E., Choi, S.H., Kawachi, Y., Mukasa, S.B. and Rogers, N.W., 2011. Evolution of pantellerite-trachyte-phonolite volcanoes by fractional crystallization of basanite magma in a continental rift setting, Marie Byrd Land, Antarctica. *Contributions to Mineralogy and Petrology*, *162*(6), pp.1175-1199. DOI: 10.1007/s00410-011-0646-z

Original Manuscript

Lowenstern, J.B., Clynne, M.A. and Bullen, T.D., 1997. Comagmatic A-type granophyre and rhyolite from the Alid volcanic center, Eritrea, northeast Africa. *Journal of Petrology*, 38(12), pp. 1707-1721. DOI: 10.1093/petroj/38.12.1707

Macdonald, R., 1974. Nomenclature and petrochemistry of the peralkaline oversaturated extrusive rocks. *Bulletin volcanologique*, 38(2), pp. 498-516. DOI: 10.1007/BF02596896

Macdonald, R., 2012. Evolution of peralkaline silicic complexes: Lessons from the extrusive rocks. *Lithos*, 152, pp. 11-22. DOI: 10.1016/j.lithos.2012.01.014

Macdonald, R., Bagiński, B. and Upton, B.G.J., 2014. The volcano–pluton interface; The Longonot (Kenya) and Kûngnât (Greenland) peralkaline complexes. *Lithos*, *196*, pp.232-241.

Mahatsente, R., Jentzsch, G. and Jahr, T., 1999. Crustal structure of the Main Ethiopian Rift from gravity data: 3-dimensional modeling.*Tectonophysics*, *313*(4), pp.363-382.

Mamo, T., 1985. Petrography and rock chemistry of well LA-8 Aluto-Langano geothermal system. Ethiopia: Auckland, New Zealand, University of Auckland Geothermal Institute.

Murphy, M.D., Sparks, R.S.J., Barclay, J., Carroll, M.R. and Brewer, T.S., 2000. Remobilization of andesite magma by intrusion of mafic magma at the Soufriere Hills Volcano, Montserrat, West Indies. *Journal of petrology*, *41*(1), pp.21-42. DOI: 10.1093/petrology/41.1.21

Mushkin, A., Stein, M., Halicz, L. and Navon, O., 2002, August. The Daly gap: low-pressure fractionation and heat-loss from cooling magma chamber. In *Geochimica et Cosmochimica Acta* (Vol. 66, No. 15 A, pp. A539-A539).

Neave, D.A., Fabbro, G., Herd, R.A., Petrone, C.M. and Edmonds, M., 2012. Melting, differentiation and degassing at the Pantelleria volcano, Italy. *Journal of Petrology*, 53(3), pp. 637-663. DOI: 10.1093/petrology/egr074

Pamukcu, A.S., Gualda, G.A., Ghiorso, M.S., Miller, C.F. and McCracken, R.G., 2015. Phase-equilibrium geobarometers for silicic rocks based on rhyolite-MELTS—Part 3: Application to the Peach Spring Tuff (Arizona–California–Nevada, USA).*Contributions to Mineralogy and Petrology*, *169*(3), pp.1-17. DOI: 10.1007/s00410-015-1122-y

Peccerillo, A., Barberio, M.R., Yirgu, G., Ayalew, D., Barbieri, M. and Wu, T., 2003. Relationships between mafic and peralkaline silicic magmatism in continental rift settings: a petrological, geochemical and isotopic study of the Gedemsa volcano, central Ethiopian rift. *Journal of Petrology*, 44(11). DOI: 10.1093/petrology/egg068

Putrika, K.D., 2008. Thermometers and barometers for volcanic systems. *Reviews in Mineralogy and Geochemistry*, 69(1), pp. 61-120.

Ren, M., Omenda, P.A., Anthony, E.Y., White, J.C., Macdonald, R. and Bailey, D.K., 2006. Application of the QUILF thermobarometer to the peralkaline trachytes and pantellerites of the Eburru volcanic complex, East African Rift, Kenya. *Lithos*, *91*(1), pp.109-124. DOI: 10.1016/j.lithos.2006.03.011

Ronga, F., Lustrino, M., Marzoli, A. and Melluso, L., 2009. Petrogenesis of a basalt-comenditepantellerite rock suite: the Boseti Volcanic Complex (Main Ethiopian Rift). *Mineralogy and Petrology*, 98(1-4), pp. 227-243. DOI: 10.1007/s00710-009-0064-3

Original Manuscript

Rooney, T.O., Bastow, I.D., Keir, D., Mazzarini, F., Movsesian, E., Grosfils, E.B., Zimbelman, J.R., Ramsey, M.S., Ayalew, D. and Yirgu, G., 2014. The protracted development of focused magmatic intrusion during continental rifting. *Tectonics*, 33(6), pp. 875-897. DOI: 10.1002/2013TC003514

Rooney, T.O., Hart, W.K., Hall, C.M., Ayalew, D., Ghiorso, M.S., Hidalgo, P. and Yirgu, G., 2012. Peralkaline magma evolution and the tephra record in the Ethiopian Rift. *Contributions to Mineralogy and Petrology*, 164(3), pp. 407-426. DOI: 10.1007/s00410-012-0744-6

Ryan, W.B., Carbotte, S.M., Coplan, J.O., O'Hara, S., Melkonian, A., Arko, R., Weissel, R.A., Ferrini, V., Goodwillie, A., Nitsche, F. and Bonczkowski, J., 2009. Global multi-resolution topography synthesis. *Geochemistry, Geophysics, Geosystems*, *10*(3).

Samrock, F., Kuvshinov, A., Bakker, J., Jackson, A. and Fisseha, S., 2015. 3-D analysis and interpretation of magnetotelluric data from the Aluto-Langano geothermal field, Ethiopia. *Geophysical Journal International*, *202*(3), pp.1923-1948. DOI: 10.1093/gji/ggv270

Scaillet, B. and Macdonald, R., 2001. Phase relations of peralkaline silicic magmas and petrogenetic implications. *Journal of Petrology*, *42*(4), pp.825-845. DOI: 10.1093/petrology/42.4.825

Scaillet, B. and Macdonald, R., 2003. Experimental constraints on the relationships between peralkaline rhyolites of the Kenya Rift Valley. *Journal of Petrology*, *44*(10), pp.1867-1894.

Siebert, L., and Simkin, T., 2002, Volcanoes of the world: An illustrated catalog of Holocene volcanoes and their eruptions: Smithsonian Institution Global Volcanism Program Digital Information Series GVP-3.

Stock, M.J., Humphreys, M.C., Smith, V.C., Isaia, R. and Pyle, D.M., 2016. Late-stage volatile saturation as a potential trigger for explosive volcanic eruptions. *Nature Geoscience*, *9*(3), pp.249-254. DOI: 10.1038/ngeo2639

Tait, S., Jaupart, C. and Vergniolle, S., 1989. Pressure, gas content and eruption periodicity of a shallow, crystallising magma chamber. *Earth and Planetary Science Letters*, *92*(1), pp.107-123. DOI: 10.1016/0012-821X(89)90025-3

Teklemariam, M., 1996. Water–rock interaction processes in the Aluto-Langano geothermal field, Ethiopia. *Plinius*, (15-16), p. 161.

Teklemariam, M., Battaglia, S., Gianelli, G. and Ruggieri, G., 1996. Hydrothermal alteration in the Aluto-Langano geothermal field, Ethiopia. *Geothermics*, 25(6), pp. 679-702. DOI: 10.1016/S0375-6505(96)00019-3

White, J.C., Parker, D.F. and Ren, M., 2009. The origin of trachyte and pantellerite from Pantelleria, Italy: insights from major element, trace element, and thermodynamic modelling. *Journal of Volcanology and Geothermal Research*, 179(1), pp. 33-55. 70 DOI: 10.1016/j.jvolgeores.2008.10.007

Wilks, M., 2016, A Seismological Investigation into Tectonic, Magmatic and Hydrothermal Processes at Aluto and Corbetti, Two Restless Volcanoes in the Main Ethiopian Rift. (Doctoral dissertation, University of Bristol).

Wright, T.J., Ebinger, C., Biggs, J., Ayele, A., Yirgu, G., Keir, D. and Stork, A., 2006. Magma-maintained rift segmentation at continental rupture in the 2005 Afar dyking episode. *Nature*, *442*(7100), pp.291-294.

Original Manuscript

Yimer, M., 1984, The petrogenesis, chemistry and hydrothermal mineralogy of rocks in the Langano Aluto geothemal system, Ethiopia, Unpublished report, Geothermal Institute, University of Auckland, pp. 75.

Younger, P.L., 2014. Missing a trick in geothermal exploration. *Nature Geoscience*, *7*(7), pp.479-480. DOI: 10.1038/ngeo2193

Original Manuscript

FIGURE CAPTIONS

Figure 1 – *Topographic map of the East African Rift system. Map was generated in GeoMapApp (Ryan et al., 2009; http://www.geomapapp.org/). The locations of the Main Ethiopian Rift, and the Kenyan Rift to the south, are identified by the solid and dashed black lines. Red dashed lines indicate the divisions between the SMER, CMER, NMER and Afar region (after Corti., 2009). Volcanic centres (data from the Smithsonian Global Volcanism Program; Siebert and Simkin, 2002) are represented by the small grey triangles. Aluto, located in the CMER, is represented by the larger red triangle.*

Figure 2 – *Photomicrographs (a, b, d, e) and electron backscatter images (c, f) of representive basaltic and pantelleritic samples from Aluto. (a-c) Images from basaltic sample 17-01-05. (a) Subophitic texture is shown, indicating that the plagioclase grew before or contemporaneously with the clinopyroxene phenocryst. (b) Large clinopyroxene phenocryst displaying reverse zoning (confirmed by SEM imaging), only two of these phenocrysts are present in the sample and are hence volumetrically minor. (c) Electron backscatter image of olivine phenocrysts displaying Fe rich rims (indicated by the lighter colours on the back scatter image). (d, e) Granophyric texture present in sample 01-02-14, seen here with an alkali feldspar core. (f) Electron backscatter image of aenigmatite phenocryst in sample 30-01-10. Scale bars in all images represent 500 μm except panel f where the scale bars represents 100 μm.*

Figure 3 – *modal proportions of phenocryst phases in pantelleritic lavas from Aluto. Dominant phases are alkali feldspar and quartz. Apatite is also present in some samples, but is generally an accessory phase, forming <1% of the phenocryst population.*

Figure 4 – *Graphs displayed explain the advantage of the aWSR method over the mWSR method, and why using >15 points for the aWSR analysis my give erroneous results. Both graphs show hypothetical liquid lines of descent. Starting composition for these hypothetical models is represented by the black dot, and the 'target' composition (i.e. the composition of the natural samples) is marked by the shaded green area. (a) For the two separate models, the point recorded by the mWSR analysis is represented by the red dot. It would appear from the mWSR analysis that Model 2 most closely approached the 'target' region. However, when the entire area considered by the aWSR analysis (blue region of line) is taken into account, it is clear that Model 1 overall provides the better match to the target region. (b) At low melt fractions (f<0.1) some models using Rhyolite-MELTS fail to converge. This leads to a bias in the aWSR analysis, as models that are able to progress to low melt fractions are more likely to pass through the entire range of the target region. This results in better match as data points with low residuals either side of the target region are analysed (Model 2). For models that do not progress to low melt fractions (Model 1), data points only on one side of the target region are analysed, which will result in a higher aWSR value. To limit this effect, the aWSR analysis is confined to only the minimum 15 data points of each model.*

Figure 5 – *Liquid line of descent generated by Rhyolite-MELTS and the composition of natural samples from Aluto are shown. Black line represents the changing melt composition during fractional crystallisation under the best fit conditions according to the aWSR analysis. The point at which olivine (Ol); Clinopyroxene (Cpx); Plagioclase (Plag); Spinel (Spl); Apatite (Apa); Rhombohedral-Oxide (Rhm-oxide); and Sanidine (San) begin to precipitate are indicated in each graph. It can be seen that Rhyolite-MELTS does not accurately reproduce the FeO_t, P_2O_5 or CaO content of the pantelleritic samples. (e) dashed lines show degree of crystallisation in 20% intervals.*

Figure 6 – *Graphs show the dominant phases that are predicted to form during fractional crystallisation. These results are shown for a range of storage conditions which all have low residuals in the aWSR analysis. (b) represents the best fit conditions as determined by the aWSR analysis. Vertical dashed black line represents the temperature of H_2O saturation in each particular model.*

Original Manuscript

Figure 7 – *Liquid lines of descent showing the influence of changing oxygen fugacity. The best match to the compositional data from Aluto appears to be achieved at $fO_2 = QFM - QFM+1$. Labels on panel **c** show the mineral-in points from plagioclase feldspar and spinel under conditions of $fO_2 = QFM-2$. Panel **d** show the spinel-in points for conditions of $fO_2 = QFM$ and $QFM+1$, and the rhm-oxide-in point for $fO_2 = QFM+1$. Panel **e** shows the spinel-in points for all models apart from those with $fO_2 = QFM-2$. It can be that spinel saturation occurs at a later stage of fractional crystallisation as the fO_2 drops.*

Figure 8 – *Liquid lines of descent showing the influence of pressure at 1 wt% initial H_2O. At 0.5 wt% H_2O the effects of pressure on the liquid line of descent are shown to be minor. The major factor is the influence of pressure on the stability of the feldspars. Labels in panel **b** show that as pressure increases the sanidine-in point occurs at a lower SiO_2 concentration. Hence a poor match to the compositional data is seen at P > 150 MPa. Panel **c** shows the plagioclase-in points, indicating that this occurs at lower Al_2O_3 concentrations as pressure decreases (i.e. plagioclase is more stable at lower pressures). Finally, panel **d** shows how the formation of an Al- and Ti-rich clinopyroxene leads to a decrease in the TiO_2 content of the magma in all models at P > 50 MPa.*

Figure 9 – *Liquid lines of descent showing the influence on initial water content. Panel **a** shows a decrease in the Na_2O content of the residual magma at >65 wt% SiO_2 for models at H_2O > 1 wt%. This appears to be due to an increase in the stability of the albite end member of the feldspar ternary. Panel **c** shows the plagioclase-in point of each model, and indicates that increasing water content results in delayed formation of plagioclase. Panel **d** indicates the formation of a Ti-rich clinopyroxene in models where H_2O > 1wt%, resulting in a poor match to the composition of the basaltic and intermediate samples from Aluto.*

Figure 10 – *(a) Results of aWSR. This figure shows the effect of fO_2 on the match between the modelled composition of the residual liquid and the composition of pantellerites from Aluto. These results clearly indicate that magmas are likely to be stored at an oxygen fugacity near (or slightly above) the QFM buffer. (b) results of aWSR analysis showing the effect of pressure on the fit between the modelled residual liquid composition and the composition of peralkaline rhyolites from Aluto. These results show that the best matches are generally seen between 100 and 150 MPa, but that the lowest residuals are seen at 150 MPa when lower water contents (0.5 wt%) are invoked. (c) results of aWSR analysis showing the effects of changing water content at 100 MPa and 150 MPa. It can be seen that at higher pressures, any models with water contents above 0.5 wt% have an extremely poor match to the compositional data. At lower pressure (100 MPa) the effects of water contents are lessened, but the lowest residuals are observed near 1wt% H_2O. These results, alongside the better match to basaltic and intermediate compositions at low water contents, suggest that parental magmas beneath Aluto are likely to contain 0.5 wt% H_2O.*

Figure 11 – *Schematic diagram showing the different regions of magmatic storage indicated by InSAR and seismological investigations and the depth of storage indicated by this study. Figure adapted from Hutchison et al. (2016a). The region of most likely magma storage, identified by analysis of isobaric fractional crystallisation models in this study, is indicated on the figure. The location of the deformation source for the 2008 ground deformation event, as identified by Hutchison et al. (2016a), is located by the red dot at ~5 km depth. This is hypothesised to represent the top of a magmatic storage region. Analysis of seismic events between 2012 and 2014 by Wilks (2016) reveals a decrease in the number of recorded seismic events between 4 and 7 km depth. The number of seismic events recorded with depth is indicated by the red line. This may provide further evidence for magmatic storage at this depth.*

Original Manuscript

Figure 12 *– Variation in rate of SiO$_2$ content change with time (d[SiO$_2$]/dt) with temperature. Using the method of Mushkin et al. (2002) it is possible to calculate the rate at which the SiO$_2$ content of the magma changes during fractional crystallisation. All variables and parameters used in these calculation can be obtained from Rhyolite-MELTS apart from T$_o$, the temperature of the surrounding wall rock. We therefore use three possible wall rock temperatures in our calculations, following the method of White et al. (2009). It can be seen that the rate at which silica changes increases dramatically following spinel (and apatite) fractionation. Therefore, this indicates that the SiO$_2$ content of the magma increases rapidly through the Daly Gap region. As a result, few intermediate composition magmas are expected to be present in the magmatic reservoir.*

Original Manuscript

TABLE TITLES AND CAPTIONS

Table 1 – *whole rocks compositions of samples from Aluto and the surrounding region compiled by Hutchison et al. (2016a). All data presented here was determined by X-ray Fluorescence (XRF) analysis.*

Caption: *Samples 17-01-01G and 17-01-01K have anomalously low Na_2O values, and high LOI values. It is suggested by Hutchison et al. (2016b) that this may occur due to post-emplacement alteration of otherwise pristine pumice samples, as has previously been suggested in other studies (Fontijn et al., 2013; Peccerillo et al., 2003). Errors on the whole-rock analysis of Hutchison et al. (2016b) are reported as counting statistical errors (cse), and analysis of a USGS accepted standard was used in order to assess the data quality. Errors are summarised as the average cse for all samples analysed here: SiO_2 0.032%; TiO_2 0.002%; Al_2O_3 0.014%; Fe_2O_3 0.003%; MnO 0.001%; MgO 0.003%; CaO 0.002%; Na_2O 0.010%; K_2O 0.005%; P_2O_5 0.000%; SO_3 0.001%.*

Table 3 – *description of the method from which the 'fit' between each individual fractional crystallisation model and the composition of natural samples from Aluto is calculated.*

Table 4 – *review of previous studies that have identified the conditions of magma storage beneath peralkaline volcanic centres.*

Original Manuscript
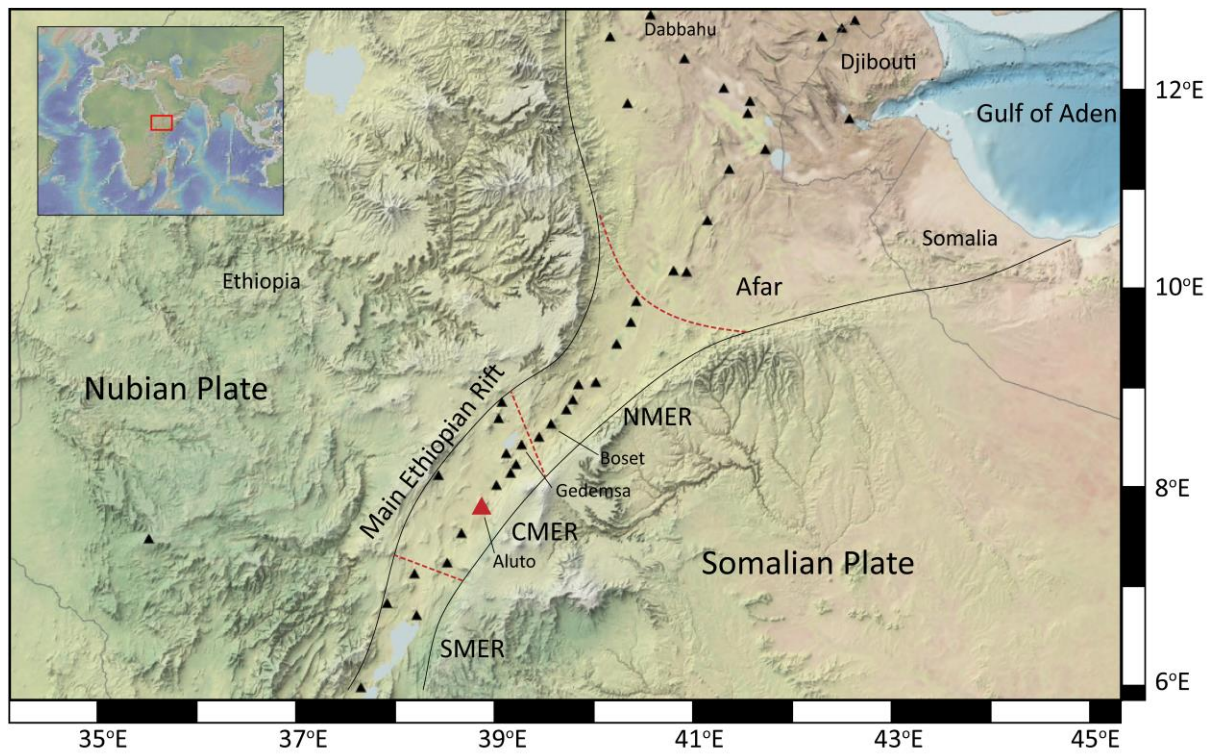
Fig. 1

Original Manuscript
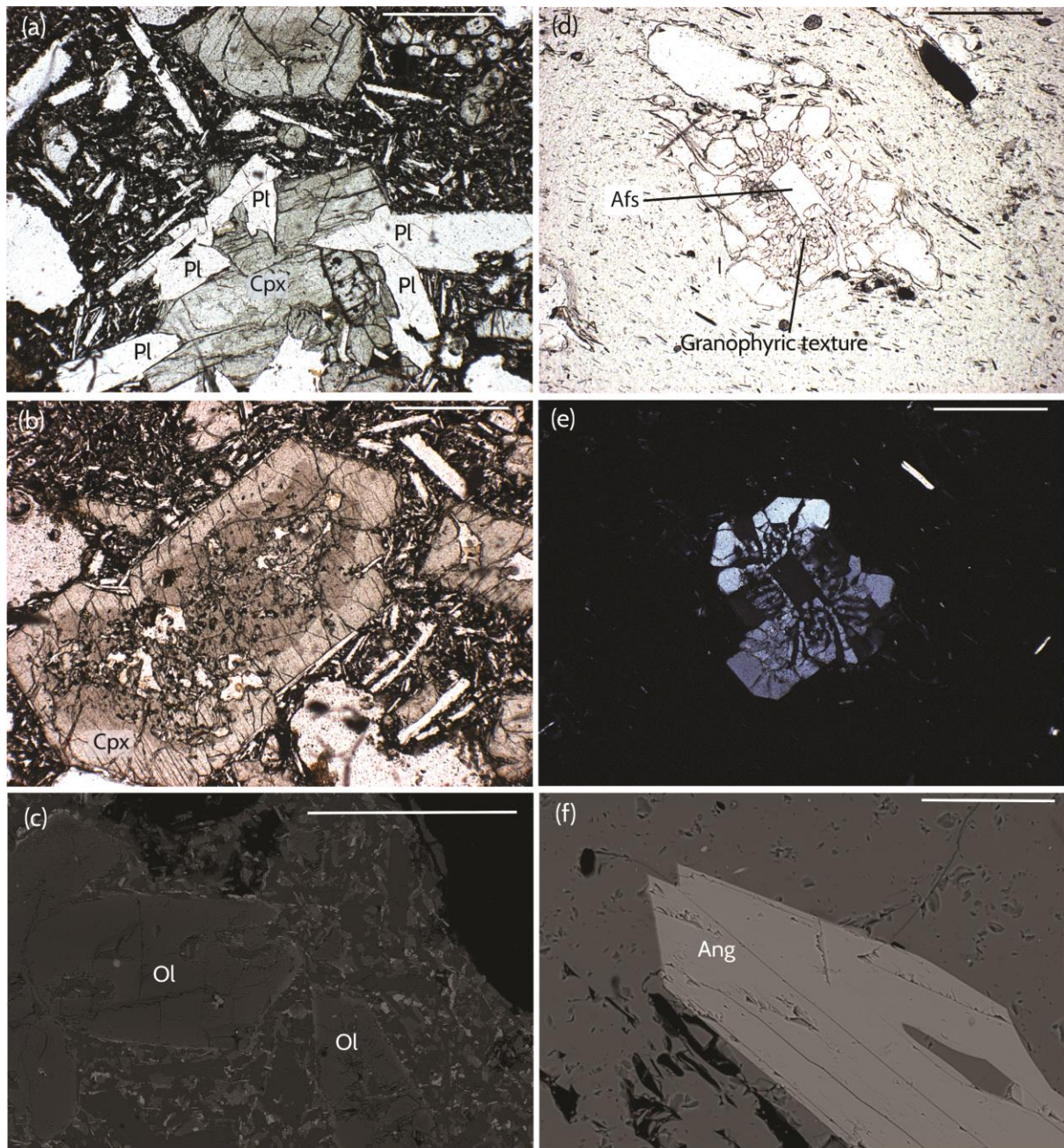
Fig. 2

Original Manuscript
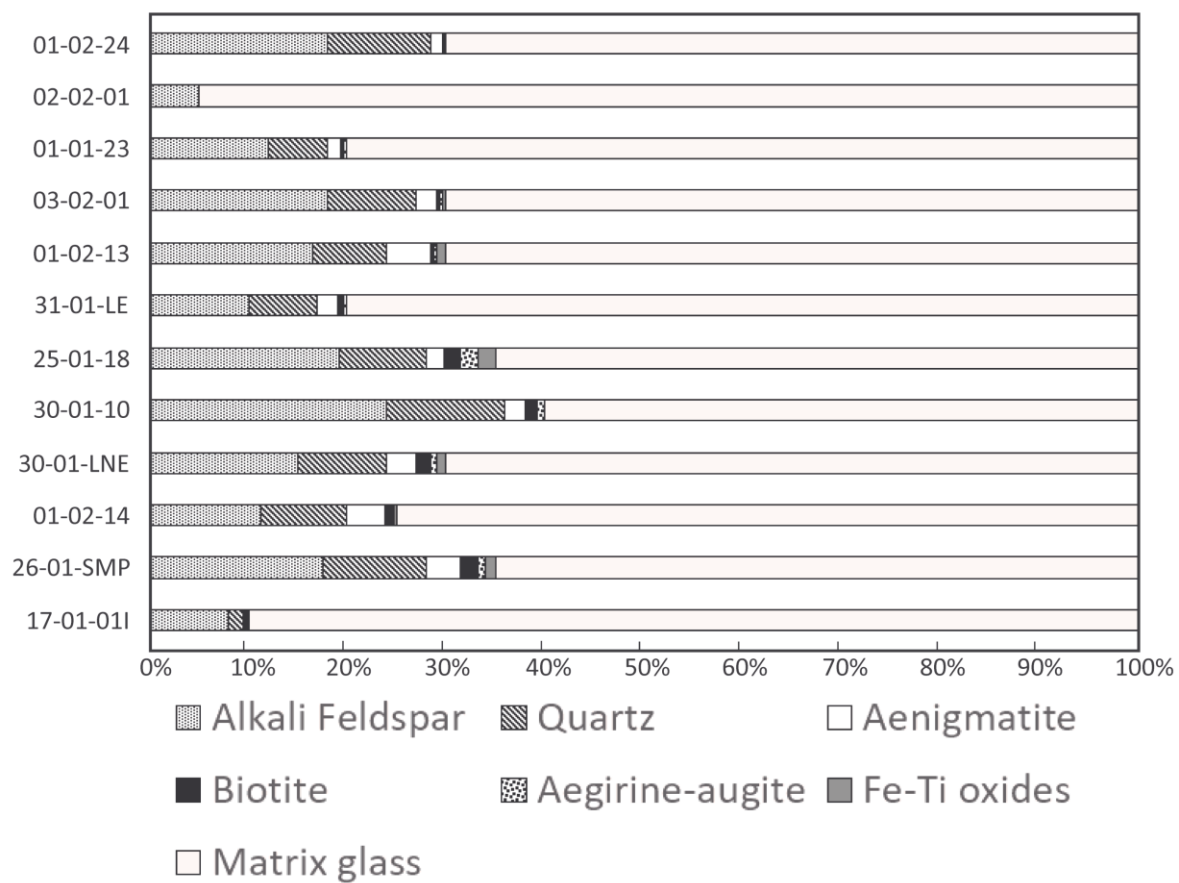
Fig. 3

Original Manuscript
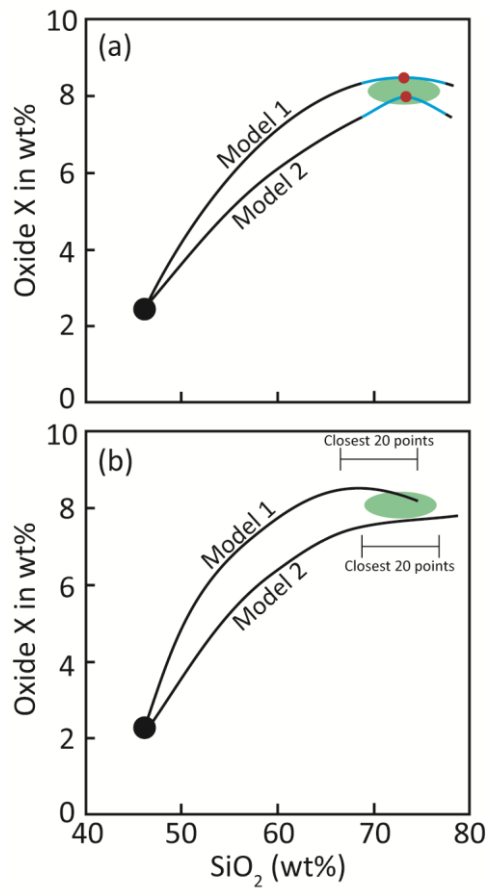
Fig. 4

Original Manuscript
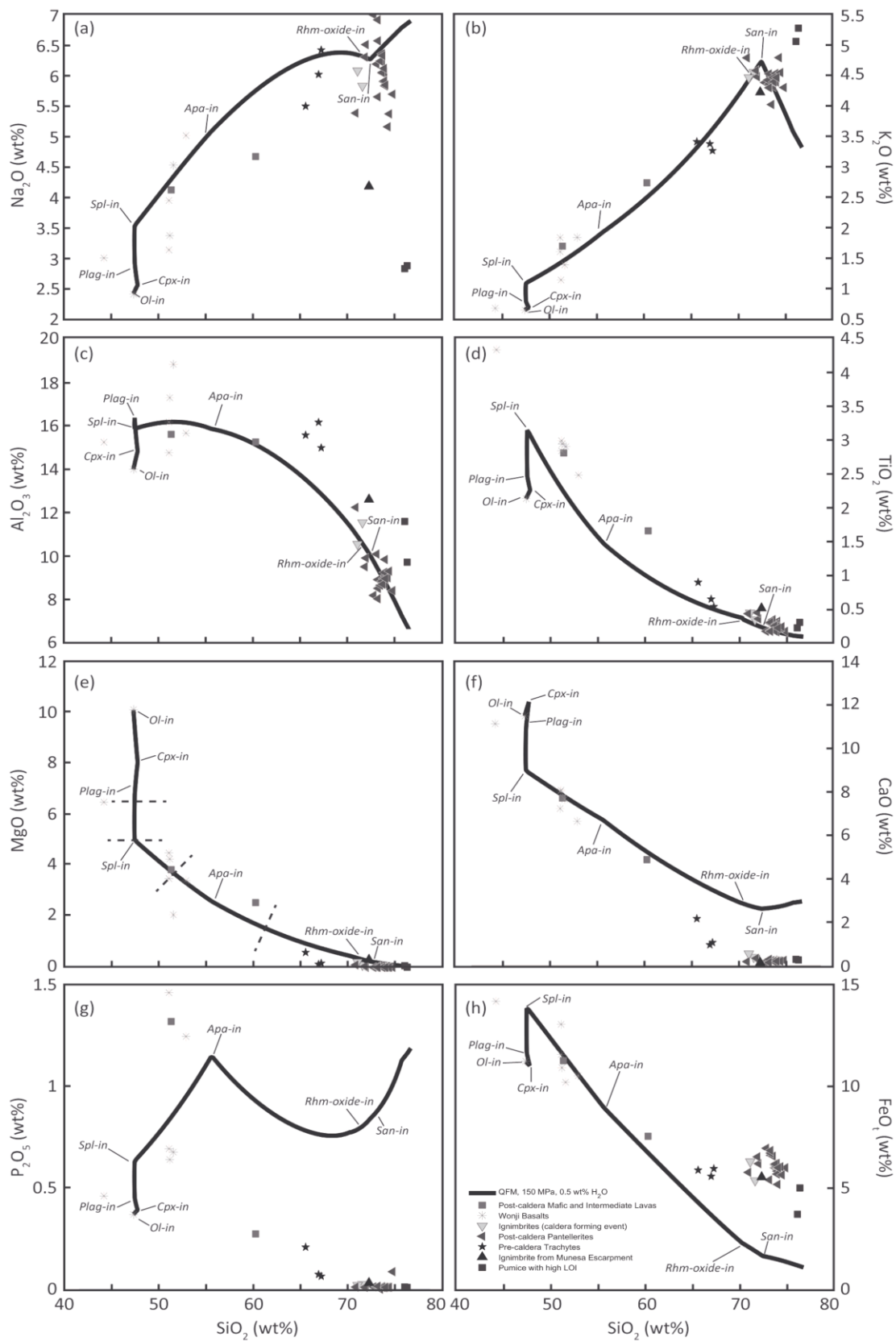
Fig. 5

Original Manuscript

Fig. 6
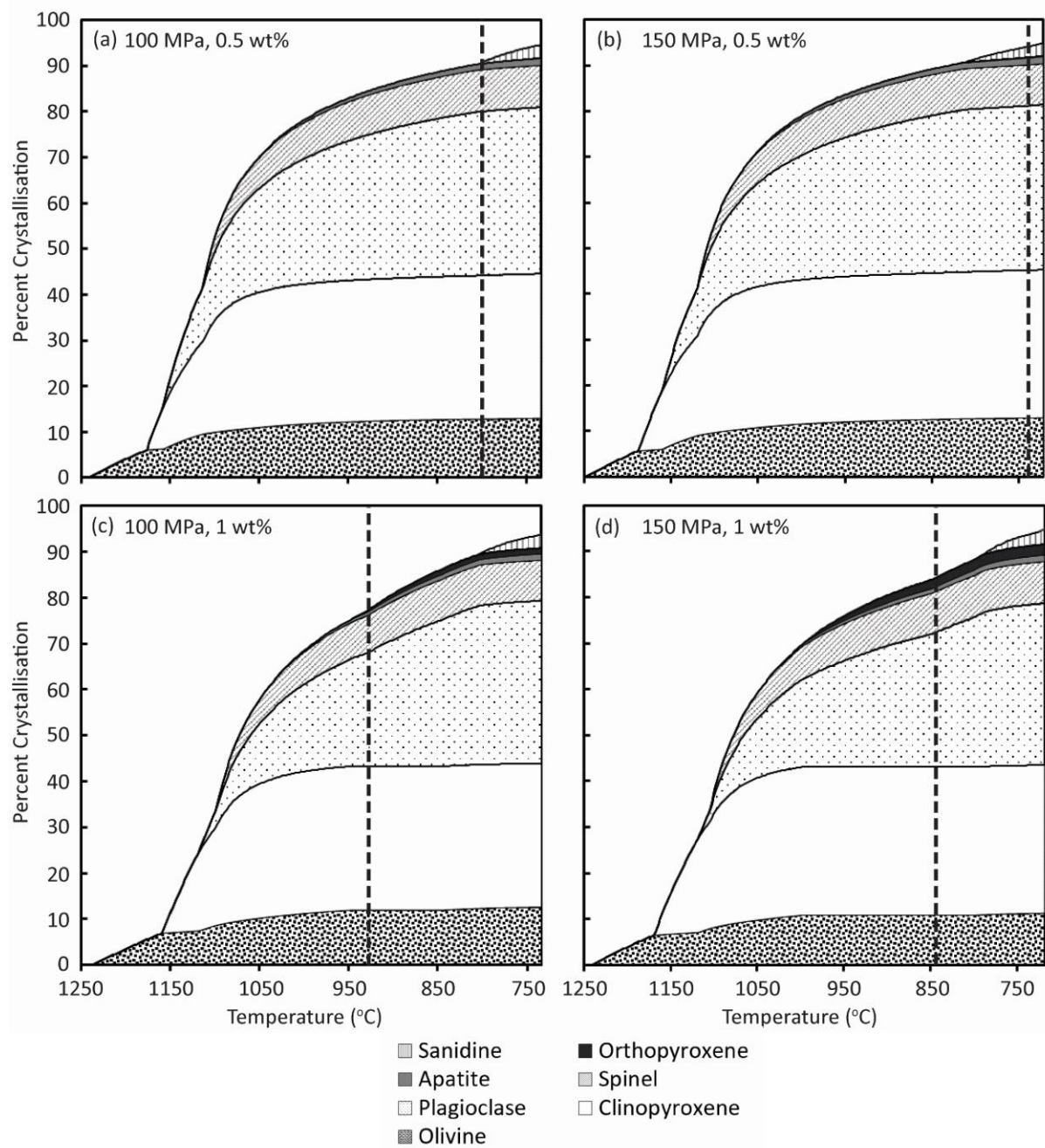
Original Manuscript
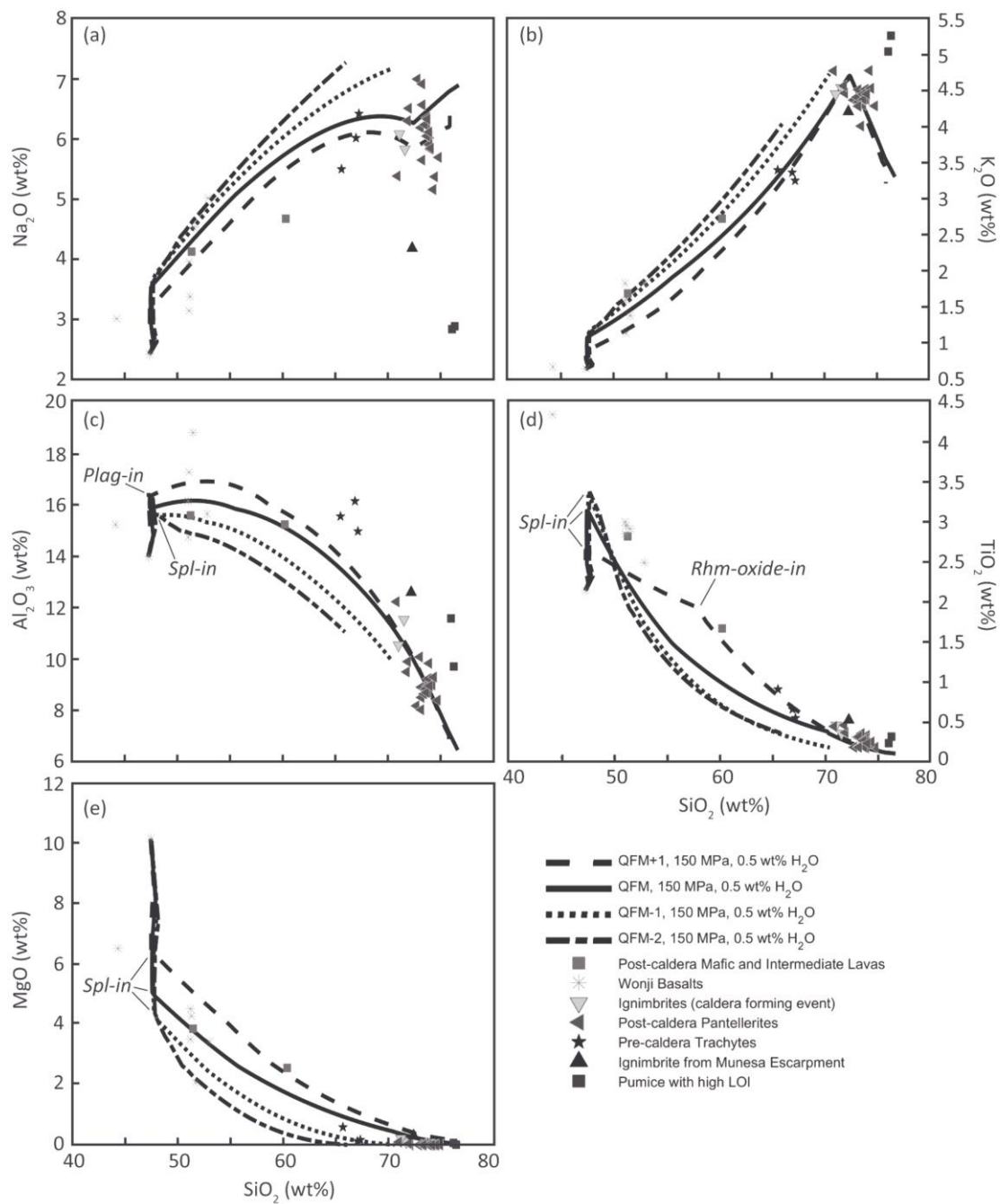
Fig. 7

Original Manuscript
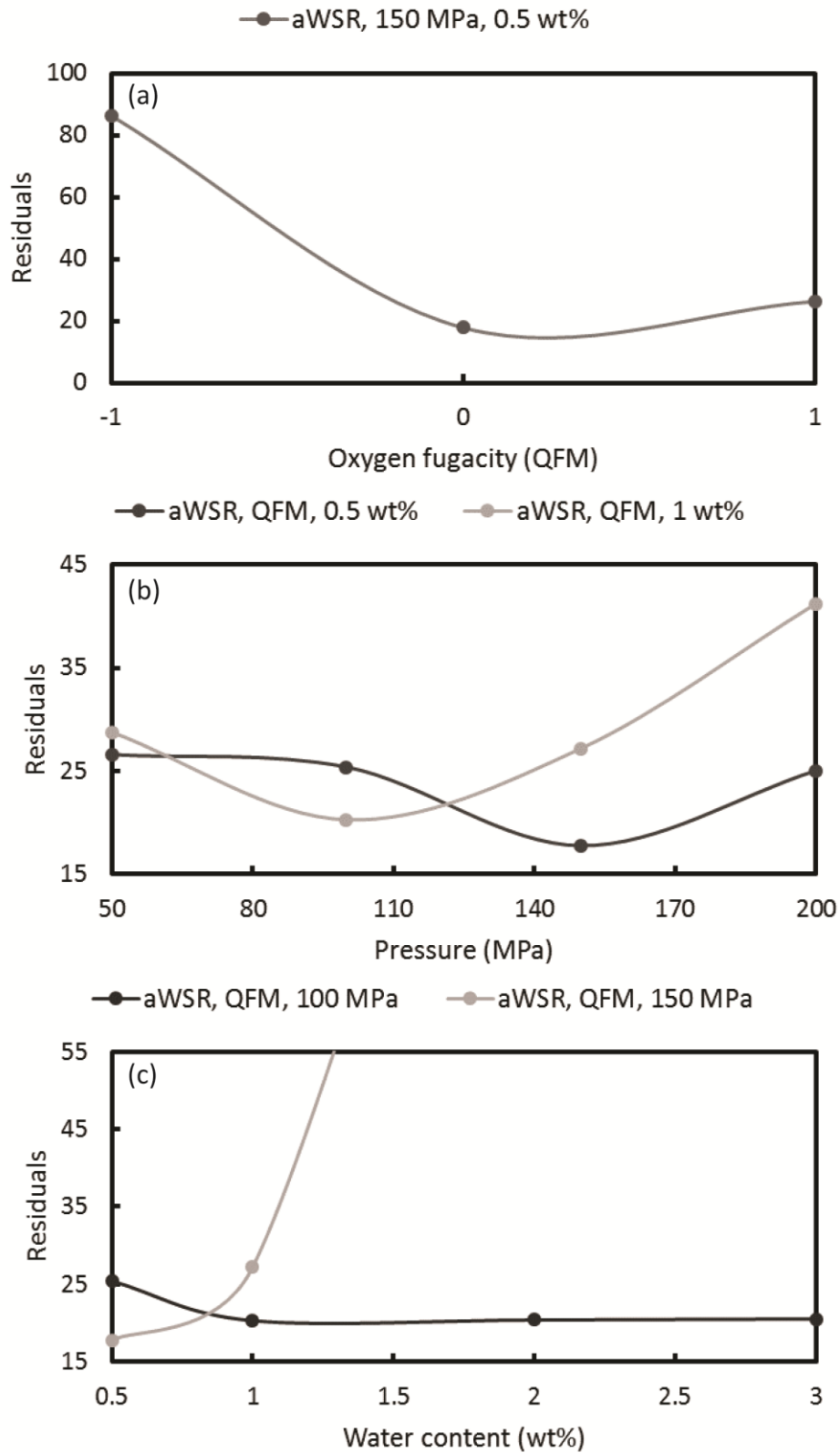
Fig. 8

Original Manuscript
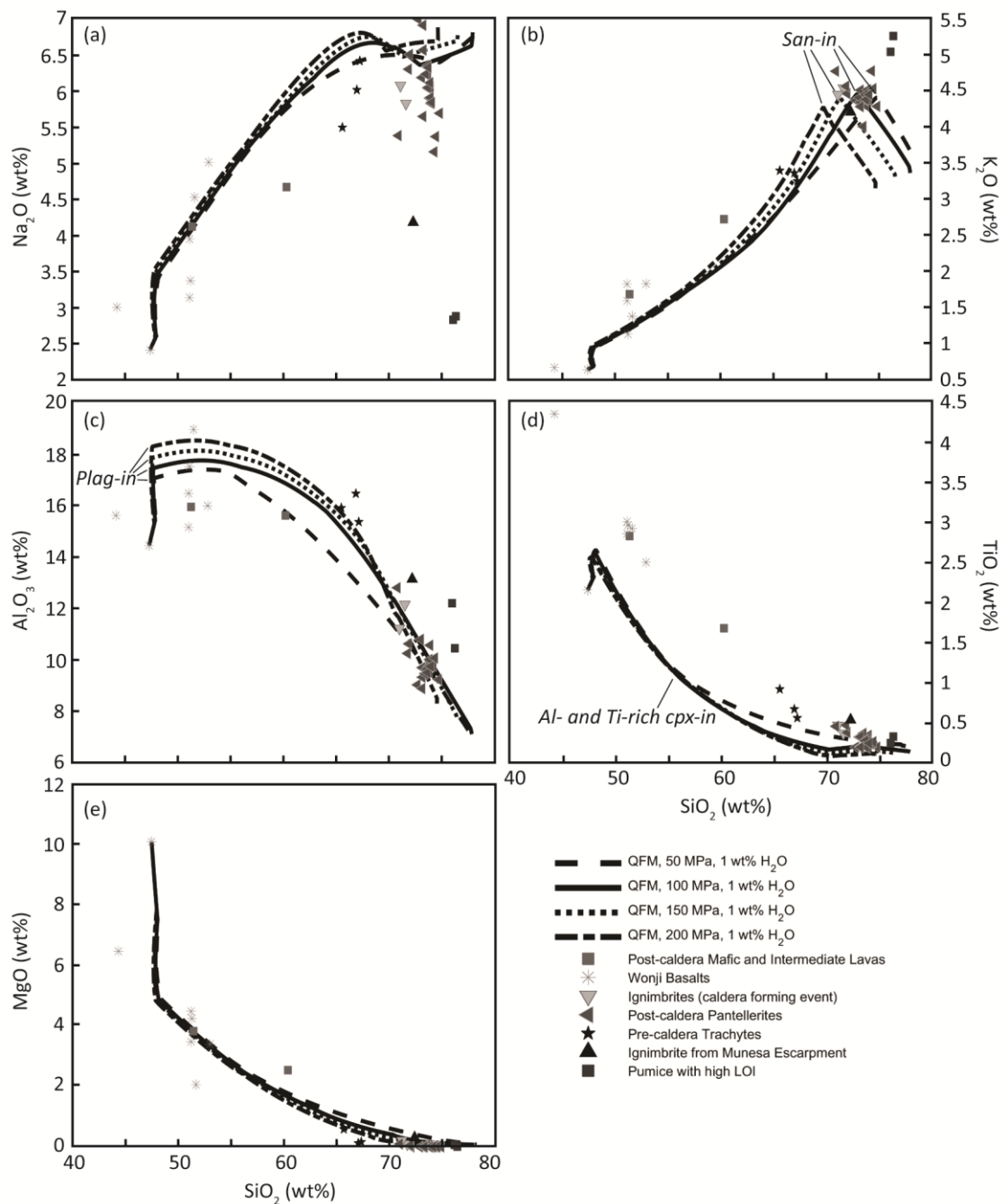
Fig. 9

Original Manuscript
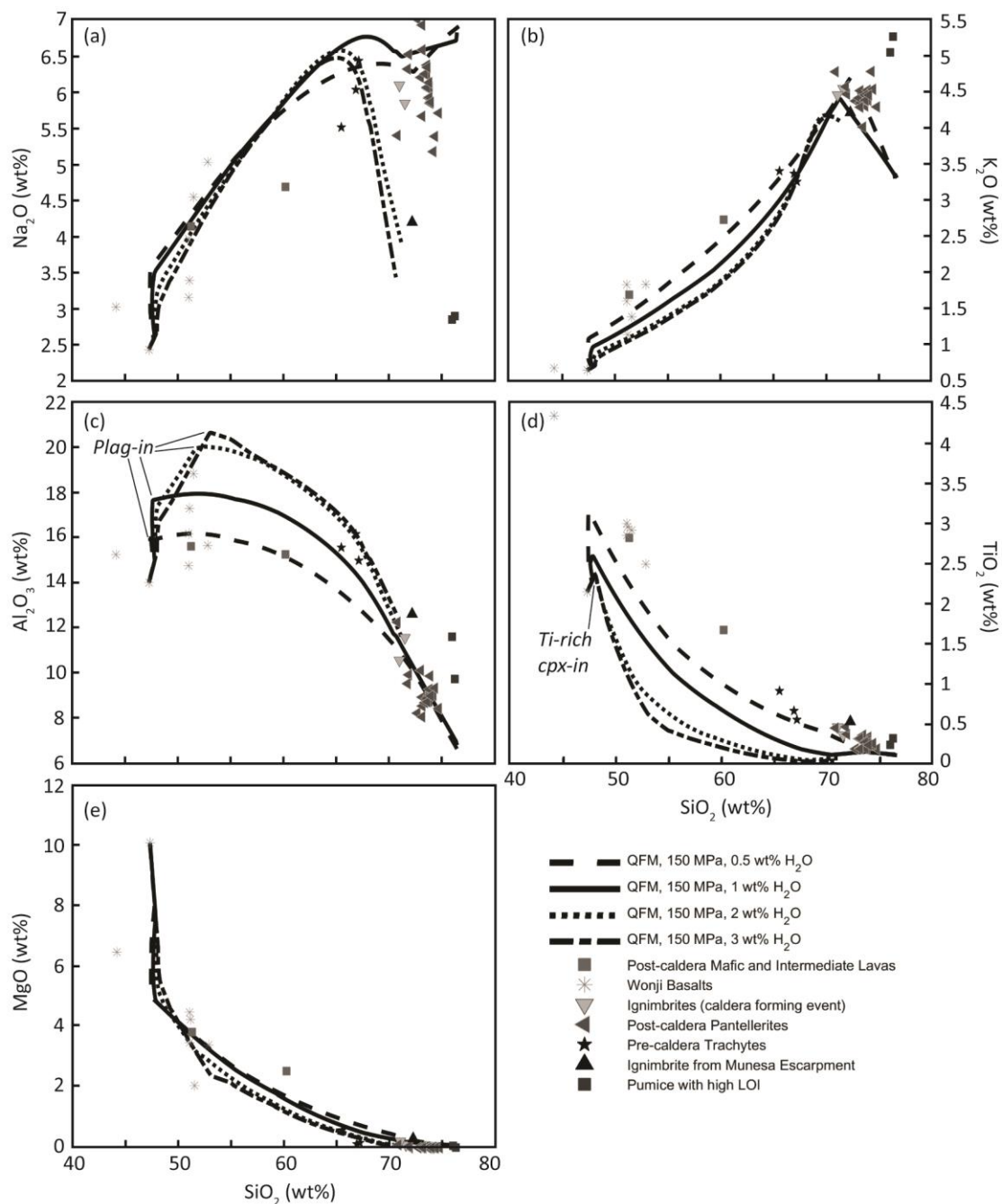
Fig. 10

Original Manuscript

Fig. 11
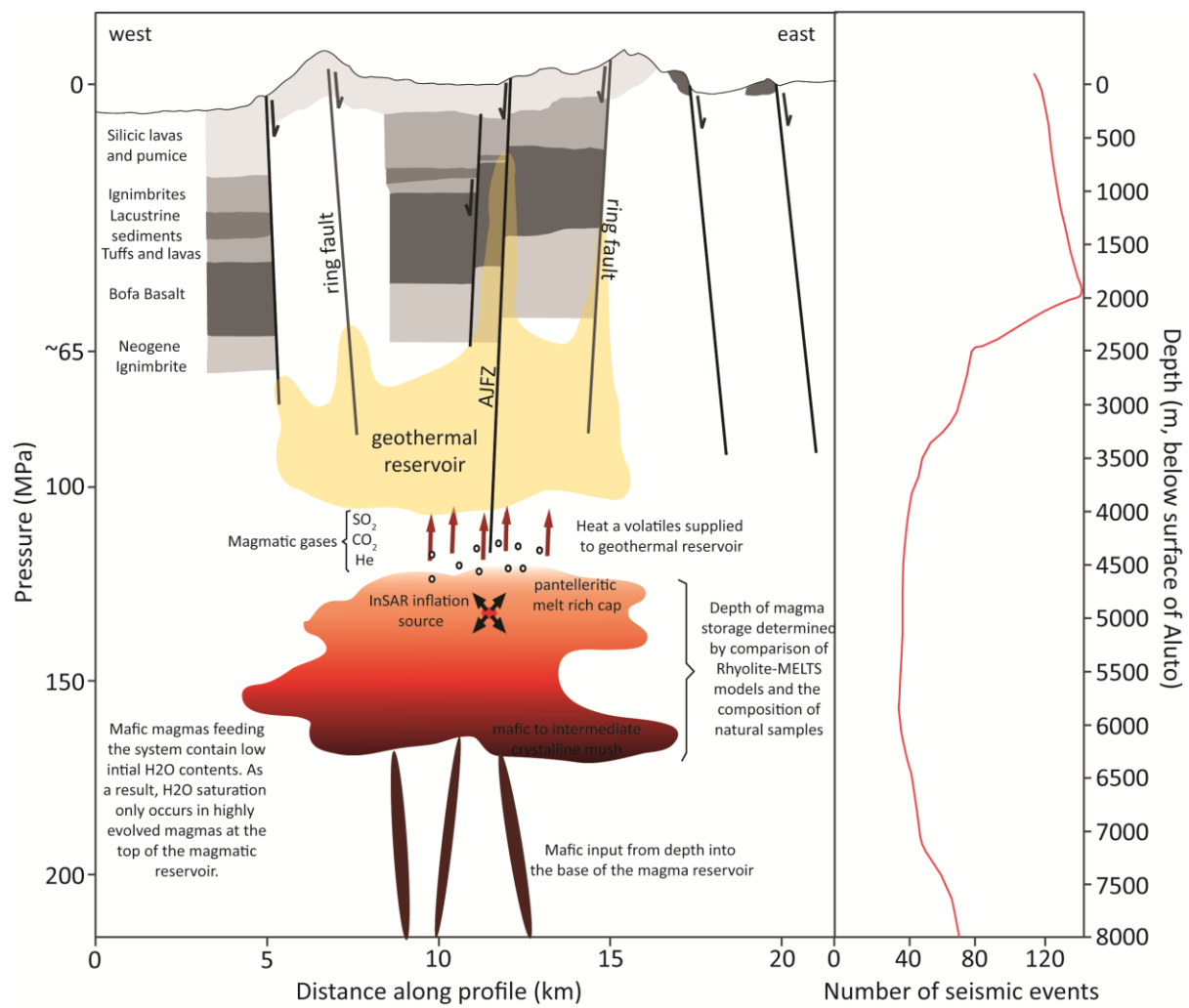
Original Manuscript
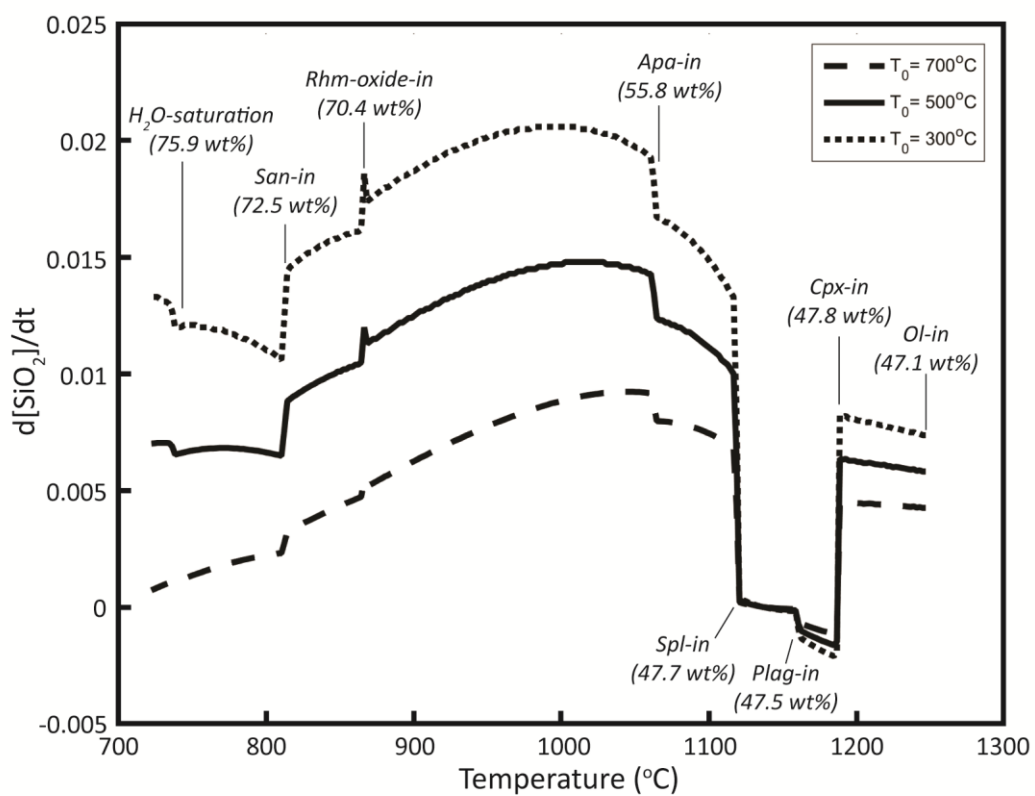
Fig. 12

Original Manuscript

Table 1 – Whole rock compositions of samples erupted at Aluto and the surrounding area, from Hutchison et al. (2016c). All data were measured by X-ray Fluorescence Spectroscopy.

Sample	Rock Type	Concentration (wt%)												
		SiO_2	TiO_2	Al_2O_3	FeO_t	MnO	MgO	CaO	Na_2O	K_2O	P_2O_5	SO_3	LOI	Total
17-01-05	Basaltic lava	46.41	2.089	13.7	12	0.185	9.95	11.24	2.37	0.627	0.361	0.009	0.98	99.92
18-11-01	Basaltic lava	50.24	2.75	15.25	12	0.262	3.77	7.54	4.03	1.649	1.29	0.024	0.49	99.29
15-01-01B	Lithic clast from PDC	52.53	2.462	15.53	11.37	0.245	3.4	6.59	4.98	1.816	1.235	<0.002	0.28	100.44
15-01-07B	Scoria	59.85	1.645	15.13	8.15	0.144	2.53	4.83	4.64	2.705	0.271	0.065	0.57	100.53
15-02-09	Trachyte lava	65.18	0.89	15.46	6.36	0.222	0.59	2.14	5.46	3.38	0.206	0.005	0.31	100.21
18-11-06	Trachyte lava	66.38	0.53	14.78	6.39	0.318	0.17	1.05	6.34	3.215	0.063	-0.007	0.76	99.98
18-11-07b	Trachyte tuff	65.92	0.64	15.9	5.97	0.1	0.12	0.94	5.92	3.315	0.072	-0.008	1.14	100.04
18-01-04	Pumice from PDC	69.37	0.289	8.44	6.92	0.287	0.04	0.28	5.35	4.277	0.013	0.011	3.67	98.95
30-01-03B	Pumice from PDC	70.74	0.241	8.49	6.46	0.262	<0.004	0.2	5.81	4.275	0.012	<0.002	3.21	99.69
18-01-11	Pumice from PDC	71.04	0.214	8.6	6.29	0.238	<0.004	0.21	4.93	4.573	0.01	0.005	3.54	99.64
30-01-01B	Pumice from PDC	71.33	0.233	8.92	5.97	0.223	<0.004	0.2	5.7	4.364	0.011	0.004	2.83	99.8
26-01-21A	Pumice from PDC	71.79	0.273	8.72	6.37	0.254	<0.004	0.23	5.74	4.319	0.009	<0.002	2.22	99.92
02-02-03	Pumice from PDC	71.83	0.173	8.48	6.54	0.272	<0.004	0.19	6.17	4.268	0.01	0.007	1.91	99.84
02-02-02	Pumice from PDC	72.25	0.164	8.52	6.6	0.275	<0.004	0.19	5.98	4.289	0.009	<0.002	2.04	100.31
30-01-06B	Pumice from PDC	72.41	0.233	9.05	5.98	0.223	<0.004	0.2	5.22	4.41	0.01	<0.002	2.19	99.92
16-01-05	Pumice from PDC	72.43	0.168	8.14	6.31	0.261	0.01	0.24	5.51	4.155	0.084	<0.002	2.68	99.99
27-01-03	Pumice airfall	70.61	0.286	10.3	5.71	0.21	<0.004	0.25	5.45	4.387	0.009	<0.002	2.65	99.87
03-02-23	Pumice airfall	70.86	0.167	7.78	7.2	0.324	<0.004	0.14	6.69	4.147	0.014	<0.002	2.14	99.47
17-01-01K	Pumice from tuff cone	71.46	0.211	10.8	3.78	0.134	0.07	0.27	2.66	4.739	0.011	<0.002	5.68	99.9
17-01-01G	Pumice from tuff cone	72.03	0.289	9.17	5.14	0.184	0.01	0.25	2.72	4.968	0.008	<0.002	5.15	99.91

Original Manuscript

Sample	Description													Total
03-02-28	Pumice cone	71.34	0.215	8.63	6.28	0.239	<0.004	0.19	5.63	4.292	0.01	0.008	3.16	100
18-02-04	Aphanitic rhyolite lava	70.02	0.43	12.08	6.2	0.19	0.1	0.18	5.32	4.719	0.011	-0.01	0.82	100.05
02-02-01	Aphyric obsidian	70.71	0.352	9.73	6.63	0.275	<0.004	0.28	6.4	4.391	0.016	<0.002	-0.32	98.46
02-02-12	Aphyric obsidian	72.68	0.3	10.03	5.84	0.22	<0.004	0.24	6.15	4.389	0.011	<0.002	-0.22	99.65
01-02-14	Porphyritic obsidian	71.3	0.171	8.02	7.41	0.318	<0.004	0.18	6.86	4.284	0.011	<0.002	-0.29	98.26
26-01-SMP	Porphyritic obsidian	71.77	0.279	8.69	6.38	0.254	<0.004	0.25	5.87	4.281	0.01	<0.002	1.94	99.72
01-02-24	Porphyritic obsidian	72.7	0.18	8.44	7.13	0.296	<0.004	0.2	6.52	4.315	0.01	<0.002	-0.21	99.58
18-01-08	Porphyritic obsidian	73.15	0.222	8.88	6.48	0.246	<0.004	0.2	6.31	4.274	0.009	<0.002	-0.04	99.74
01-02-13	Porphyritic obsidian	73.3	0.243	8.79	6.65	0.268	<0.004	0.2	6.19	4.352	0.01	<0.002	-0.17	99.83
30-01-LNE	Porphyritic obsidian	73.36	0.245	8.99	6.29	0.236	<0.004	0.2	6.01	4.359	0.009	<0.002	-0.14	99.56
31-01-LE	Porphyritic obsidian	73.56	0.318	9.78	5.59	0.216	<0.004	0.22	5.8	4.353	0.009	<0.002	-0.4	99.45
13-05-04	Welded ignimbrite	71.13	0.34	11.46	5.8	0.219	0.1	0.39	5.79	4.514	0.025	-0.001	0.22	100
15-01-07A	Silicic enclave within scoria cone	72.85	0.341	10.84	5.79	0.213	0.12	0.32	5.41	4.187	0.026	<0.002	0.19	100.27
Following data is from Di Paola (1972)														
DP4	Scoriaceous boulder	42.38	4.15	14.59	14.8	0.21	6.24	10.65	2.88	0.64	0.44	2.24	-	99.22
DP34	Aphyric obsidian	70.45	0.44	9.32	6.97	0.36	0.05	0.33	6.18	4.48	0.01	3.74	-	102.33
DP35	Aphyric obsidian	72.23	0.34	8.51	7.01	0.38	0.04	0.23	6.13	3.94	0	0.91	-	99.72
Following data is from Teklemariam (1996) and Teklemariam et al. (1996)														
S-1	Ignimbrite (Munesa escarpm	70.21	0.5	12.23	5.85	0.17	0.3	0.13	4.06	4.09	0.03	1.91	-	99.48

Original Manuscript

	ent)													
S-2	Coarsely porphyritic basaltic lava	49.76	2.86	16.79	11.56	0.17	4.15	7.83	3.28	1.1	0.62	1.49	-	99.61
S-3	Grey welded ignimbrite	69.92	0.44	10.37	6.74	0.27	0.21	0.54	5.98	4.38	0.02	0.68	-	99.55
Following data is from Yimer (1984) and Mamo (1985)														
ETH-A12	Coarsely porphyritic basaltic lava	50.45	2.84	18.4	10.87	0.17	2.03	7.48	4.43	1.35	0.66	0.56	-	99.24
ETH-A13	Aphyric basaltic lava	50.08	2.78	14.44	13.93	0.26	3.43	7.07	3.87	1.79	1.43	0.01	-	99.09
Mamo-1494	Porphyritic basaltic lava	48.04	2.81	15.18	11.84	0.2	4.24	7.52	2.95	1.5	0.65	3.43	-	98.36

Caption/footnote of Table 1: *Samples 17-01-01G and 17-01-01K have low Na_2O and high LOI values, which may reflect post-emplacement alteration of otherwise pristine pumice (Hutchison et al., 2016c), as identified in studies of other volcanic systems (Fontijn et al., 2013; Peccerillo et al., 2003). Uncertainty on the whole-rock analyses of Hutchison et al. (2016c) are reported as counting statistical errors (cse) and analysis of a USGS standard was used to assess the data quality (see Hutchison et al., 2016c for details). Average cse for samples used in this study are: SiO_2 0.032%; TiO_2 0.002%; Al_2O_3 0.014%; Fe_2O_3 0.003%; MnO 0.001%; MgO 0.003%; CaO 0.002%; Na_2O 0.010%; K_2O 0.005%; P_2O_5 0.000%; SO_3 0.001%.*

Original Manuscript

Table 2 – *Magma storage conditions investigated in Rhyolite-MELTS models, the range of values used and the intervals over which they were varied. The range of model input variables are constrained based on previous studies of peralkaline magma systems as cited in the table.*

Parameter	Range	Interval	Previous constraints
Pressure (MPa)	50 to 300	50	Experimental work of Caricchi et al. (2006) has shown that peralkaline rhyolites cannot be generated from fractional crystallisation of a transitional basaltic parent at pressures above 0.5 GPa. Hence, lower pressure conditions are investigated.
Oxygen Fugacity (log units relative to the Quartz-Fayalite-Magnetite buffer)	-2 to +1	1	Macdonald (2012) suggests that peralkaline magmas commonly have an fO_2 between QFM-1 and QFM. This is supported by the results of White et al. (2005) which suggested the oxygen fugacity of peralkaline rhyolites from Pantelleria lie near the QFM buffer.
Water Content (wt%)	0.5, 1 to 3	1	White et al. (2009) found that initial water contents in transitional basaltic parental magmas are likely to be around 1.5wt% H_2O, resulting in peralkaline rhyolite with 4-6wt% H_2O pre-eruption. This is supported by measured concentrations of H_2O in basalts (0.9-1.6 wt%) and pantellerites (up to 5 wt%) from pantelleria (Giocada and Landi, 2010; Neave et al., 2012). Field et al. (2012) indicated that lower initial water contents (<1 wt%) may be present in parental magmas for peralkaline rhyolites.

     Corresponding Author Email: mlmg3@cam.ac.uk

Original Manuscript

Table 3 – *Summary of magma storage conditions identified previously in peralkaline volcanic systems and comparison with the storage conditions at Aluto identified in this study*

Volcano	Region	Relevant study	Method	Storage conditions and comments
Aluto	CMER	This study	MELTS	'Best fit' storage conditions are identified to be: fO_2 = QFM; P = 150 MPa; initial H_2O = 0.5 wt%.
Boseti	NMER	Ronga et al. (2010)	MELTS	Composition of eruptive products are reproduced by thermodynamic modelling at 100 MPa, 1 wt% H_2O, fO_2 = QFM.
Gedemsa	NMER	Peccerillo et al. (2003)	MELTS	Composition of eruptive products are reproduced by thermodynamic modelling at 50 MPa, 1 wt% H_2O, fO_2 = QFM.
Dabbahu	Afar	Field et al. (2012; 2013)	Melt inclusions; InSAR; seismics; Fe-oxide oxybarometry	Shallow storage (stacked sills) at 1-5km b.s.l. hypothesised deeper storage (14-20 km depth) where bulk of magmatic differentiation occurs. Low water content <1wt% (MgO = 9 wt%) and fO_2 = QFM.
Pantelleria	Straits of Sicily	White et al. (2005; 2009); Di Carlo et al. (2010)	MELTS; QUILF; Fe-oxide oxybarometry	Composition of trachytic magmas can be generated by fractional crystallisation models at 100 MPa, 1 – 1.5 wt% H_2O (MgO = 6 wt%), fO_2 = QFM-1. Additionally, QUILF equilibria and Fe oxide pairs indicate crystallisation near the QFM buffer for highly peralkaline magmas. Finally, experimental results are consistent with crystallisation at 5 ± 1 km depth.
Eburru	Kenyan peralkaline province	Ren et al. (2006)	QUILF	Calculated temperatures of 700-708°C and fO_2 = QFM – 1.6 to +0.5.
Olkaria	Kenyan peralkaline province	Scaillet and Macdonald (2001)	Experimental analysis on comenditic samples	Experiments indicate that phenocryst assemblages crystallised at fO_2 ~ QFM, T = 660 - 740°C, and P = 50 - 150 MPa.
Bursey; Andrus; Kosciusko	Marie Byrd Land, Antarctica	LeMasurier et al. (2011)	Comparison of phonolitic and pantelleritic lavas and consideration of phase stability	Polybaric processes may be important, but the final stages of pantellerite evolution is likely to take place at <5 km depth, which favours fractionating a high plagioclase/clinopyroxene ratio increasing the peralkalinity of a magma.
Furnas	São Miguel, Azores	Jeffery et al. (2016)	MELTS	P = 150 MPa, fO_2 = QFM, initial H_2O = 1.5 wt% (MgO = 10 wt%).

Corresponding Author Email: mlmg3@cam.ac.uk

Original Manuscript

Highlights:

- Isobaric crystallisation can reproduce the compositional diversity seen at Aluto.

- The magma storage conditions at Aluto are: fO_2=QFM; P=150 MPa; initial H_2O=0.5 wt%.

- Inferred magma storage depth is consistent with modelling of ground deformation.

- Magma storage conditions are comparable to those at other peralkaline volcanoes.